

Author Version of : CATENA, vol.228; 2023; Article no: 107154

## Acquisition of Natural Remanence in the basaltic laterites of Deccan Volcanic Province (India): Implications to Palaeomagnetic studies in laterites

N. B. Kadam<sup>1,5</sup>, S. J. Sangode<sup>1,\*</sup>, M. Venkateshwarlu<sup>2</sup>, D C Meshram<sup>1</sup>, Y R Kulkarni<sup>3</sup>, Firoz Badesab<sup>5</sup>, Jyotibala Singh<sup>1</sup>, S. S. Gudadhe<sup>4</sup>

1: School of Earth Sciences, Savitribai Phule Pune University, Pune 411 007 (India)

2: CSIR-National Geophysical Research Institute, Hyderabad (India)

3: Department of Civil Engineering, Gharda Institute of Technology, Khed, Ratnagiri (India)

4: Yashwantrao Chavan Arts, Commerce and Science College, Lakhandur (India)

5: CSIR-National Institute of Oceanography, Panaji, Goa (India)

\*Email of Corresponding author: sangode@rediffmail.com

### Abstract

Lateritization in the Deccan basalt province (India) represents a large spectrum of chemical weathering with up to 99% of CIA values and the complete ferri- to antiferromagnetic transformations. We combined rock magnetic, palaeomagnetic, XRD, and XRF analyses to investigate the mineralogical transformations and its relationship to the acquisition of natural remanent magnetization (NRM) by sampling a 25 m thick Deccan lateritic profile from the West Coast of India. Significant amount of amorphous hematite (*ha*), crystalline hematite (*hc*), goethite and their Al- substituted forms were detected along with gibbsite and kaolinite. The domain size association of 'SP+SD and 'SP+SD+MD' in the ferri- as well as antiferromagnetic forms; and combination of *ha* and *hc* yield strong NRMs amongst these laterites. Low field demagnetization (< 5mT) allows removal of *ha*<sub>NRM</sub>; and the secondary components due to ferrimagnetic oxides can be removed at <25 mT. Thereafter, the *hc*<sub>NRM</sub> continued to decay up to >150 mT. Palaeomagnetic tests (Koenisberger ratio, MDF, intensity decay and Zijderveld diagrams) indicate stable Characteristic remanent magnetizations (ChRM) due to *hc*; and the Al-substitutions does not affect the ChRM stability, depicting these laterites as excellent palaeomagnetic recorders. The stable ChRMs due to Chemical/Crystallization RMs due to '*hc*' also benchmarks the degree of maturity within the process of lateritization.

**Keywords:** Laterite, Mineralogy, Rock magnetism, Deccan basalt, Palaeomagnetism.

## 1. Introduction

Laterites are the manifestations of deep, prolonged, and intensive chemical weathering that occurred on differing host lithologies (Widdowson and Cox, 1996; Bourman and Ollier, 2002; Wimpenny et al., 2007, Ollier and Seth, 2008, Babechuk et al., 2014, Ghosh et al., 2015). Selective diminution of alkali, alkaline earth elements, and silica from parent rock through the process of lateritization results in gradual enrichment of the iron and aluminium oxides and hydroxides along with some residual clays (Widdowson and Gunnell, 1999; Borger and Widdowson, 2001; Widdowson, 2007).

Widespread occurrence of laterites is observed in tropical regions particularly during the Cenozoic period (Bardossy, 1981; Gunnell, 2003). Laterites from the Indian subcontinent particularly preserve a variety of processes from different ages and host rocks (Meshram and Randive, 2011; Caner et al., 2011). Some of the pioneering and fundamental information on laterites is also derived from the Indian west coast occurrences (Buchanan, 1807) and were studied using physical, geochemical (Widdowson and Cox, 1996; Kiskurek et al., 2004; Babechuk et al., 2014, 2015; Suhr et al., 2018) and mineral magnetic perspective (Liu et al., 2019; Singh et al., 2020).

The prolonged process of lateritization permits sufficient time for NRM acquisition depicting them as good magnetostratigraphic recorders. However, there is ambiguity in understanding the acquisition in terms of the lateritization process. A single lateritic profile can be perceived through different superimposing processes dominated by solution and precipitation activities (Widdowson, 2007; Babechuk et al., 2014, Suhr et al., 2018). Palaeomagnetic studies in lateritic profiles therefore demand detailed mineralogical assessment in context to NRM acquisition. The renewed interest in basaltic laterites as possible analogues of Martian weathering processes (Hynek et al., 2002; Landis et al., 2004; Thomas et al., 2005; Greenberger and Mustard, 2012), CO<sub>2</sub> sequestration during basaltic weathering (Seifritz, 1990; Schuiling and Krinjgsman, 2006; Gislason and Oelkers, 2014) further demand detailed studies from ideal basaltic laterites, such as the Deccan traps. Iron oxides being the chief constituent of laterites, magnetic mineralogy and spectroscopy makes some of the most suitable approaches for such investigations.

The basalts are enriched with ferrimagnets and hence provide a complete spectrum of transformation to antiferromagnetic oxides during through the process of lateritization. The complex nature of lateritization allows many repeated and superimposed reaction series of partial to complete oxidation, hydroxylation, dissolution, and precipitation leading to the processes such as maghematization, ferry-hydroxylation, Al-substitution, crystallization, and recrystallization. Several

residual, crystalline, and amorphous minerals are produced during lateritization compelling the use of multiple spectroscopic and magnetic approaches to analyse the laterites. On the other hand, it enriches our understanding on NRM acquisition by chemical/crystallization remanent magnetizations (CRMs). This study is aimed at finding the efficacy of NRM in terms of palaeomagnetic signatures from the laterites.

The mineral/rock magnetism is a well-established approach for identification of different phases of iron oxides enabling their semi-quantitative estimates (Thomson and Oldfield, 1986, pp. 21-38; Evans and Heller, 2003, pp. 50-78; Liu et al., 2012). Intensive work has been made to delineate and differentiate dominant phases of ferrimagnetic mineralogy (i.e. magnetite, maghemite, and greigite) from the antiferromagnetic minerals. Further the studies are available to provide distinction within the antiferromagnetic phases (e.g., Dekkers and Rochette, 1992; France and Oldfield, 2000; Sangode and Bloemendal 2004; Roberts et al., 2020; Jiang et al., 2022). The antiferromagnetic minerals can carry stable remanence over a longer period makes them suitable for palaeomagnetic studies (Dunlop and Ozdemir, 1997, pp. 16-42; Roberts et al., 2020). Previously, Schmidt et al. (1983) made palaeomagnetic attempts on Indian laterites and found considerable scatter in data which he then inferred mixing of normal and reverse magnetization demanding detailed mineralogical studies. Substitution of cations (e.g., Al) and amorphous to crystalline transformations within antiferromagnetic complexes (Cornell and Schwertmann, 2003, pp. 39-57; Liu et al., 2007; Hu et al., 2016) is a crucial factor in the determination of magnetic properties akin to the standard and theoretical values. Laterites being highly enriched with antiferromagnetic oxides/hydroxides such as hematite, goethite, ferrihydrites and lepidocrocite (Kisakurek et al., 2004; Meshram and Randive, 2011; Babechuk et al., 2014, 2015; Suhr et al., 2018; Singh et al., 2020) provide an opportunity to study the complex processes and their implications on NRM. Here we characterized the lateritic magnetic minerals, their concentration and domain sizes to understand its implications on NRM acquisition.

## **2 Study Area**

The Indian subcontinental drift from the southern to northern hemisphere continued until its collision with Asia to form the Himalayas (Klootwijk and Pierce, 1979; Courtillot et al., 1988). During this transect voluminous lavas were erupted at ~65 Ma ago around the Cretaceous-Tertiary (K-T or K-Pg) boundary, occupying an area of 500,000 km<sup>2</sup>, thus creating the Deccan traps (Klootwijk and Pierce, 1979) as large igneous province. This formed the substrate for the lateritization typically under the tropical humid conditions over suitable geomorphological surfaces. The studied laterites are formed over the Poladpur Formation of Deccan traps. The thickness of lava flows belonging to the Poladpur Formation varies from 3 to several 10's of meters spread over wide distances (Duraishwami et al., 2014).

The studied laterites occur on the Konkan plain are known as low-level laterites (Widdowson and Cox, 1996) and are depicted in the Fig. 1a. Schimdt et al. (1983) divided Indian laterites into late Cretaceous-early Tertiary laterites and mid-to-late Tertiary laterites.

### 3. Materials and methods

Large oriented block samples ( $>30 \text{ cm}^3$ ) of laterites were collected at 5m intervals from the freshly excavated laterites near the Chiplun area covering an entire profile of 25 m. Sample 1 and sample 7 are from the top and bottom of the profile, respectively. Samples of the fresh host basalt were obtained at the base of the profile for mineralogic and palaeomagnetic reference. All the samples were cored into standard specimen sizes keeping the orientations in-tact and the sets of palaeomagnetic and rock magnetic studies were prepared. For instance, specimens of sample number 1 are labelled 1.1, 1.2, 1.3, etc. for palaeomagnetic measurements, and 1A, 1B, 1C for rock magnetic measurements.

#### 3.1 Rock magnetic measurements

Magnetic susceptibility was measured using Bartington MS2B susceptibility meter operated dual frequency ( $\chi_{lf}$  at 0.465 and  $\chi_{hf}$  at 4.65 kHz). The  $\chi_{fd}$  and  $\chi_{fd} \%$  were calculated using  $(\chi_{lf} - \chi_{hf})$  and  $[(\chi_{lf} - \chi_{hf})/\chi_{lf}] \times 100$ , respectively. Anhysteretic remanent magnetization (ARM) was induced by a peak AC field of 200 mT superimposed over 0.1 mT DC bias field using Magnon alternating field demagnetizer (Germany). The values for susceptibility of ARM ( $\chi_{ARM}$ ) were calculated by normalization of ARM with DC bias field. Isothermal remanent magnetization (IRM) was imparted using ASC-IM-10-30 (USA) impulse magnetizer. The field was induced at incremental steps from 25 to 2200 mT and backfields from -10 to -1000 mT. The magnetizations were measured using Molspin (Minispin) magnetometer (Sensitivity:  $3 \times 10^{-5} \text{ A/m}$ ), whereas the palaeomagnetic remanence was measured using the JR-6A spinner magnetometer (AGICO, Czech) (Sensitivity:  $2.4 \times 10^{-6} \text{ A/m}$ ). The maximum field available in the laboratory (i.e., 2200 mT) was considered as saturation field to calculate the SIRM (Evans and Heller, 2003, pp. 50-78). The values of susceptibilities and remanent magnetizations throughout the calculations were mass normalized. Table 1 (Supplementary file) summarizes the parameters used for estimation of different parameters and Table 2 (Supplementary file) accounts the mean values of the studied parameters. Backfield data were used to calculate the coercivity of remanence ( $B_{CR}$ ). Rock magnetic and palaeomagnetic analyses were carried out at the Palaeomagnetic laboratories of Department of Geology, Savitribai Phule Pune University (SPPU) and the CSIR- National Geophysical Research Institute, Hyderabad.

### 3.2 Hysteresis loops and thermomagnetic measurements

Set of samples were analysed for thermomagnetic, XRF and XRD studies using standard methods. Hysteresis loops and thermomagnetic curves were generated on advanced variable field translation balance (AVFTB) (Sensitivity-  $5 \times 10^{-5}$  Am<sup>2</sup>/kg, Temperature window- 0 to 800°C) at CSIR- NGRI. The hysteresis loop parameters were analyzed using software 'rockmagalyzer' (<https://earthref.org/RockMagAnalyzer/>).

### 3.3 X-ray fluorescence (XRF)

A set of powdered samples (six samples of laterite and two samples of basalt) were used for XRF analyses to calculate the weathering indices. The analyses were made on ED-XRF SPECTRO XEPOS III unit at SPPU following the sample preparation procedure described in Kisakurek et al (2004). USGS standards AGV-1, BHVO-1, VL-1 and VL-2 were used as standards for calibration (LaBrecque and Schorin, 1987). The geochemical indices were calculated using spreadsheet provided by Babechuk et al (2014). Chemical index of alteration (CIA) and Mafic index of alteration (MIA)(oxidation) were measured using moles of oxides in their formulae, while oxide wt % were used in the case of the index of lateritization (IOL) with formulae given below.

$$\text{CIA} = [\text{Al}_2\text{O}_3 / (\text{Al}_2\text{O}_3 + \text{CaO} + \text{Na}_2\text{O} + \text{K}_2\text{O})] \times 100$$

$$\text{MIA} = [(\text{Al}_2\text{O}_3 + \text{Fe}_2\text{O}_{3(\text{T})}) / (\text{Al}_2\text{O}_3 + \text{Fe}_2\text{O}_{3(\text{T})} + \text{MgO} + \text{CaO} + \text{Na}_2\text{O} + \text{K}_2\text{O})] \times 100$$

$$\text{IOL} = [(\text{Al}_2\text{O}_3 + \text{Fe}_2\text{O}_{3(\text{T})}) / (\text{SiO}_2 + \text{Al}_2\text{O}_3 + \text{Fe}_2\text{O}_{3(\text{T})})] \times 100$$

### 3.4 X-ray diffraction (XRD)

RIGAKU XRD Model ULTIMA IV was used to generate the XRD spectra for bulk powder samples from each unit at SPPU. The 2θ scan range was set at 10 to 80° with a step interval of 0.02° and speed of 4 per second. Samples were measured in Cu-Kα mode applying a voltage of 45 KV and the intensity of 40 mA. Phase identification and refinement were accomplished using Match software (<http://www.crystalimpact.com/match/>) having options for library data search to enable the mineral identifications in the bulk samples.

## 4 Results and discussion

### 4.1 Rock magnetism

The magnetic susceptibility ( $\chi_{\text{lf}}$ ) variation within the profile (Fig. 2a and Table 2) shows values from 31 to 105  $\times 10^{-8}$  m<sup>3</sup>/kg in *Zone I*, 2 to 40  $\times 10^{-8}$  m<sup>3</sup>/kg in *Zone II*, and 77 to 84  $\times 10^{-8}$  m<sup>3</sup>/kg in *Zone III* from top to bottom. The overall range of values for *Zone I* and *III* are substantially higher than that

for *Zone II* depicting possible ferrimagnetic influence for the former compared to antiferromagnetic nature of mineralogy in *Zone II*. The  $\chi_{fd}$ % (approximate concentration of SP grains) is higher in *Zone II* relative to *Zone I and III* (Fig. 2b). The *Zone II* values range from 0.4 to 5.5%, whereas the average values for  $\chi_{fd}$ % in *Zone I and III* are 0.5 and 0.8%. Lateritization process favours a large-scale transformation within magnetic mineralogy by dissolution and precipitation in an oxidative regime of Eh-pH conditions. The  $\chi_{fd}$  % represents the effect of viscosity at room temperature for the superparamagnetic (SP) domain fraction with diameters less than 3-50 nm. The behaviour of SP grains is largely dependent on temperature and the time span of observation (O'Reilly, 1984, pp. 58-97). The  $\chi_{fd}$ % enrichment amongst *Zone II* samples suggests its formation possibly by intense dissolution-solution-precipitation activity during lateritization. The ferrimagnetic SP may arise by the dissolution of larger ferrimagnetic grains or simply by maghemitization. Whereas, *Zone II* is marked by the highest coercivities ( $B_{CR}$ ) and hard isothermal remanent magnetizations (HIRM) (described below) suggest the possible antiferromagnetic nature of the SP fraction. The intense antiferromagnetic transformations in laterites lead to the formation and precipitation of ferrihydrite and limonitic complexes in their amorphous states and nanoforms to produce the SP.

The  $\chi_{ARM}$  is generally related to the concentration of stable single domain (SSD) ferrimagnetic grains (Maher, 1988; Egli and Lowrie, 2002). As seen in Fig. 2c, the  $\chi_{ARM}$  is strikingly lower in *Zone II* compared to *Zone I and III*, with *Zone III* representing higher concentration of SSD grains of ferrimagnetic nature. The Saturation Isothermal Remanent Magnetization (SIRM) collectively depends upon the coercivity of magnetic mineral phases (Thompson and Oldfield, 1986, pp. 21-38). Magnetically hard minerals (high coercivity and low remanence) resist the applied field while soft minerals (low coercivity and high remanence) align easily along external fields. The SIRM in *Zone I* (max: 0.84 Am<sup>2</sup>/kg) and *III* (max: 0.46 Am<sup>2</sup>/kg) show exceptionally higher values than *Zone II* (Fig. 2d). SIRM values for *Zone I and Zone III* thus indicate a dominant contribution from ferrimagnetic minerals e.g. magnetite/titanomagnetite and maghemite; while *Zone II* indicates majority of antiferromagnetic complexes (hematite, goethite, and their substitutes). The SIRM values for *Zone I* are much higher than *Zone III* depicting significant ferrimagnetic contribution from magnetite-maghemite phases.

The S-ratio depict relative abundance of soft versus hard magnetic minerals (King and Channel, 1991). Theoretically, the values close to '1' correlate well with soft ferrimagnetic minerals like magnetite and prevailing lower values correspond to magnetically hard minerals such as hematite and goethite. In the present scenario, *Zone I and III* show the S ratios close to 0.9 implying dominant ferrimagnetic mineralogy (Fig. 2e). The maximum and minimum values are observed in *Zone II* and

are within the range from 0.67 to 0.02 suggesting minor contribution of ferrimagnetic minerals in overall antiferromagnetic assemblage (Fig. 2e). However, the use of S-ratio for relative contribution is statistically non-linear and the interpretation is based on their non-unique nature (Heslop, 2009).

The SIRM/ $\chi_{lf}$  ratio broadly delineates the changes in domain-size; and in the present case, it is sensitive to changes in the magnetic mineral phases along with a possible contribution from paramagnetic minerals (predominantly the clay minerals). In *Zone II*, the combination of SIRM/ $\chi_{lf}$  and  $\chi_{ARM}/\chi_{lf}$  depict bimodal distribution due to smaller and larger SD grains (Fig. 2f, 2g). The higher values of  $\chi_{ARM}/\chi_{lf}$ , a grain size indicator depict relative enrichment of SD particles and its lower values show a bias towards SP or Multidomain (MD) particles (Liu et al., 2012).

The HIRM and Soft IRM ratios are primarily inferred for discrimination of bulk concentration of ferrimagnetic and antiferromagnetic mineralogy (Robinson, 1986; Thompson and Oldfield, 1986, pp. 21-38). Overall, the high HIRM in *Zone II* indicated the predominance of antiferromagnetic minerals relative to *Zone III* (Fig. 2h). The Soft IRM values in *Zone II* are 17 times lower than *Zone III* suggesting the relative abundance of hematite and/or goethite like mineral phases (Fig. 2j). The coercivity of remanence ( $B_{cr}$ ) is a complex parameter that depends upon mineralogy, domain states, and crystal structures (Dunlop and Ozdemir, 1997, pp. 133-140). The substitution of Al or Ti in the structures of magnetic minerals however causes drastic changes in the magnetic properties (Liu et al., 2007; Liu et al., 2012). This may result in an increase or decrease in the values of saturation magnetization, coercivity, and Neel/Curie temperatures (Liu et al., 2007). The  $B_{cr}$  values are higher in *Zone II* (max- 575) than *Zone I* and *Zone III* (Fig. 2i). Nonetheless,  $B_{cr}$  in *Zone I* is twice as higher as *Zone III*. Low S-ratio, high  $\chi_{lf}$ , and SIRM along with high  $B_{cr}$  values thus indicate the existence of both antiferromagnetic and ferrimagnetic minerals in *Zone I*. Liu et al. (2007) suggested constancy of L-ratio to reflect the absolute changes in the concentration of hematite or goethite,. For conventional use of S-ratio and HIRM, therefore we estimated the L-ratio. The values were uniform in *Zone I* and *II*, attesting the fair usage of S-ratio and HIRM (Fig. 2k).

Finally, the inferences from routine mineral magnetic analysis are summarized below.

- 1) The topmost *Zone I* is dominated by an equitable proportion of soft and hard magnetic minerals with a significant concentration of SD grains. The surficial ferrimagnetic inputs can be attributed to secondary/detrital processes as described in Singh et al (2020).
- 2) The intermediate *Zone II* represents a predominant antiferromagnetic zone with minor ferrimagnetic contribution and the predominance of SP fraction. This zone mainly represents the intense lateritization with almost complete transformation of ferrimagnetic oxides along with possible addition of

antiferromagnetic complexes along with other minerals by dissolution and precipitation during intense chemical weathering enriching the antiferromagnetic oxides.

3) The lowermost *Zone III* represents a dominant ferrimagnetic mixture of SD and MD grains along with low antiferromagnetic contributions.

#### 4.2 Modelling of the isothermal remanent magnetization (IRM) spectra

When the samples are dominated by mixed magnetic mineralogy, detailed analysis of IRM curves can provide differentiation of admixtures (France and Oldfield, 2000; Liu et al., 2012). The values of acquired magnetization are plotted on the y-axis and corresponding field values on the x-axis. Fig. 3 thus depict that *Zone II* specimens are typical of antiferromagnetic nature (Dekkers and Linssen, 1989). The antiferromagnetic mineral hematite usually saturates in the fields up to 2-5 T, but the presence of goethite can increase the field of saturation up to ~6-9 T or even higher (Dekkers, 1988; Rochette et al., 2005; Liu et al., 2012). The saturation magnetization, coercivity, and Curie/Neel temperatures also depend upon the amount of substitution and degree of crystallinity (Cornell and Schwertmann, 2003, pp. 111-136; Liu et al., 2007). Thus the IRM curves for *Zone II* specimens can be subdivided into three parts depending upon the maximum magnetization induced (Fig. 3b). This proposes the variations in the mineralogy and domain size perhaps as a result of crystalline to amorphous varieties and their substitutions within the hematite dominant mineralogy along with some proportion of goethite. *Zone I* specimens show the highest enhancement compared to *Zone III*. However, *Zone III* specimens exhibit higher values of magnetization as it is dominated by ferrimagnetic minerals. This indicates a significant ferricretization in *Zone I*, while *Zone II* is dominated by lateritization.

The discrete IRM spectra are further useful for modelling the components of acquisition based upon the coercivity characters (e.g. Kruveir et al., 2001; Heslop et al., 2002; Maxbauer et al., 2016). These methods are generally applied when magnetic minerals are originated from different sources. The requirements for these methods are monotony in the data which will be achieved by increasing the IRM acquisition steps along with less magnetic interaction. As the applied field increments were less in this study, and also the magnetic minerals are grown from only one source (i.e. unimodal chemical origin), we used a plot of  $[d(M)/d(\log B)]$  against  $\log B$  (Fig. 3d, 3e, 3f) to identify mean coercivity components prior to applying further statistical procedures (e.g. smoothing, component fitting) (Tauxe et al., 1996; Maxbauer et al., 2016). The minerals that were not identified/detected by the values of coercivity from back-field application (possibly because of their lower concentration) can be separated using this plot. The plot for specimens 2A and 4C represents two coercivity



components (Fig. 3e and 3f). For specimen 2A, the mean coercivity for components 1 and 2 are 656 mT and 1413 mT, respectively (Fig. 3e). Assigning the components for specific minerals depends on the source variation (eventually which will affect the magnetic signal) (Kruveir et al., 2001; Heslop et al., 2002; Maxbauer et al., 2016).

The lateritic mineralogy being antiferromagnetic (AFM) dominant, the coercivity analysis and the rate of change of IRM acquisition (RPM) appears to have been governed by the variation within the AFM phases. IRM being an indirect method, in this lateritic composition, we anticipate these different phases as a result of substitution (e.g. Aluminium-) and the grain size variations within the range of crystalline to amorphous oxides. We further examined this mineralogy using more advanced approaches in rock magnetism and the spectroscopy (i.e., XRD). In the present case, we assign the lower values of coercivity to hematite and higher values to goethite. The significant presence of goethite apart from hematite has been confirmed using x-ray diffraction analysis (presented later). The assigned value (656 mT) of coercivity is still higher than that expected for hematite (Peters and Dekkers, 2003). As stated above, the Al-substitution increases the values of coercivity for hematite and it decreases for goethite (Roberts et al., 2006; Liu et al., 2007). Similar two components were identified for specimen 4C. However, as shown in Fig. 3f, the curve initiates with elevation (x-axis) as opposed to specimen 2A. This initial enhancement implies the influence of a small/soft ferrimagnetic (FM) component which can be attested from the rate of acquisition (RPM) plots (Fig. 3i). Furthermore, specimen 1A is dominated by only one component (i.e., FM) having a mean coercivity of 100 mT, that is in agreement with the values obtained from backfield data (Fig. 3d).

The RPM for specimen 1C shows substantial acquisition up to 500 mT, depicting magnetite-maghemite-like ferrimagnetic phases (Fig. 3g). For specimen 3C, the percentage acquisition shows two trends, one up to 300 mT and the other from 300 mT upwards (Fig. 3h). Similar results were obtained for specimen 4B. This anticipates the presence of maghemite-like phases within *Zone II*. Furthermore, it also justifies the initial peak exhibited by specimen 2A as mentioned above. We considered the possibility of maghemite (/titanomaghemites) within FM mineralogy due to the commonly occurring process of maghemitisation during weathering of magnetite/titanomagnetites sourced from the parent Deccan basalts. In a nutshell, these results indicate that *Zone II* is dominantly hematitic (Al substituted?) along with variable contributions from goethite and maghemite; and maghemite (or magnetite) is the major phase in *Zone I*.

### 4.3 Hysteresis and thermomagnetic analysis

The hysteresis curve data are plotted for representative specimens of laterite and parent rock basalt (Fig. 4). The changes in magnetization with applied fields are measured using hysteresis loops (Thompson and Oldfield, 1986, pp. 21-38). The height, width, squareness, and steepness of the hysteresis loops are the consequence of magnetic concentration, stability, ease of magnetization, and grain interactions respectively (Maher and Thompson, 1999, pp. 29-31). Also, there is a significant impact of magnetic domain size on hysteresis curves (Dunlop and Ozdemir, 1997). The laterites (Sample 2-6) typically showed wasp-waisted loops, except for Sample 1 (Fig. 4). Tauxe et al. (1996) demonstrated that the mixtures of SP and SD grains with a size range of greater than 8 nm of SP can produce wasp-waisted curves. Also, a threshold size of 15-20 nm of SP grains along with some SD grains would create an exact shape, which is exhibited in the present scenario. There is a remarkable difference between the loops from *Zone I* (Sample 1), *Zone II* (Sample 2-6) and *Zone III* (Sample 7) as expected (Fig. 4). The hysteresis loop for Sample 1 closes at lower coercivity indicating dominant ferrimagnetic mineralogy (Fig. 4a). Lower values of coercivity can be observed in Sample 7 (basalt) compared to lateritic samples indicating SD to MD magnetite grain size population in basalt (Fig. 4f; Tauxe, 2002, pp. 35-75; Liu et al., 2012).

The graph of reduced saturation remanence ( $M_{rs}/M_s$ ) against reduced coercivity ( $B_{cr}/B_c$ ) so called 'Day Plot' has been pervasively used in many studies to discriminate the grain size variations (Day et al., 1977). Here, we used the Day-Dunlop plot as modification of the Day plot (Dunlop, 2002) shown in Fig. 5. Dunlop (2002) calculated theoretical as well as actual mixing lines for magnetite domains, with modified limits of reduced ratios in the Day plot. As seen in Fig. 5, majority of the samples of laterites fall within the range of 15 and 20 nm SP-SD mixing lines with one sample falling in 10-15 nm SP-SD mixing line. This suggests varying proportion of SP and SD grains in the lateritic samples. Furthermore, it supports the illustration given for hysteresis curves. The crystallinity of hematite determines the SD threshold size (Dekkers and Linssen, 1989).

The thermomagnetic curves (Fig. 6, discussed below) indicated that the hematites are Al-substituted. The exact delineation of critical SD size of hematite is limited by substitution (Dekkers and Linssen, 1989). However, the critical SD size for hematite could possibly be elevated to 100  $\mu\text{m}$  (Kletetschka, 2002). Basalt sample is exactly falling on the mixing line of SD-MD having 15 % of MD mixtures in SD grains of magnetite (Ti). The explanation of hysteresis loops and Day-Dunlop plot suggests that the lateritic mineralogy is dominated by SP (10-20 nm) and SD AFMs. The SP fraction appears to be abundantly the amorphous hematite apart from other poorly crystalline antiferromagnetic fractions.

The identification of magnetic minerals using their respective Curie/Neel temperature has been widely used, although magnetic enhancement and diminution effects during heating/cooling often mask the recognition (Liu et al., 2004; Torrent et al., 2006; Zhang et al., 2010). Fig. 6 illustrates the heating and cooling cycles (marked by red and blue arrows) for laterite and basalt analysed using AVFTB. Sample 1 showed dramatic change in magnetization during heating (300-500°C) and a large rise during cooling, in contrast to the other laterites (Fig. 6a). The final decline in magnetization around 580°C indicates the existence of magnetite (Fig. 6a). All the remaining laterite samples show a similar pattern by sudden decrease in magnetization at 300-500°C during heating (Fig. 6b, 6c, 6d, 6e). Removal or conversion of mineral phase with higher magnetization to that with lower one possibly explains this behaviour. During the cooling cycle, we observed a significant loss of magnetization (50-80 %) concerning initial magnetization. Liu et al. (2005) observed similar changes in thermomagnetic curves for loess samples attributing such changes to conversion (inversion) of maghemite to hematite during heating in the same temperature range as observed here. They further suggested that this behaviour could also be used as an index for the presence of SP particles. The inversion temperature have been reported from 250°C to  $\geq 750^\circ\text{C}$  depending upon grain size, degree of oxidation, and incorporation of impurity to the crystal structure (Dunlop and Ozdemir, 1997) and the Neel temperature of hematite is 657°C (Dunlop and Ozdemir, 1997, p. 51). However as seen in Fig. 6, the heating curve drops around 640°C depicting the lowering of Neel temperatures due to substitution. The Al-substitution could be the most common reason for lowering of the Neel temperature of hematite (Dunlop and Ozdemir, 1997, pp. 69-74; Liu et al., 2007). The diamagnetic bias of Al substitution decreases the crystallinity of hematite eventually affecting its Neel temperature and coercivity (Cornell and Schwertmann, 2003, pp. 39-57; Liu et al., 2007).

Identification of goethite in the present case is demanding as Al-substitution, excess water and crystallinity could reduce its Neel temperature to room temperature (Dekkers, 1990; Liu et al., 2012). Also, dehydration of natural and synthetic goethite occurs at considerably lower temperatures, at less than 270°C (Lewis and Schwertmann, 1979a). Dekkers (1990) reported dehydration of goethite at the temperature range from 260 to 360°C. The basalt sample has shown a gentle decrease in magnetization up to 300°C, thereafter a small drop was observed in a temperature range of 300-400°C (Fig. 6f). Jiang et al. (2015) suggested magnetic enhancement in synthetic samples due to iron content from clay minerals and subsequent production of magnetite. There is a possibility of titanomagnetite to be exsolved into Ti-rich and Ti-poor magnetite phases at elevated temperatures (Dunlop and Ozdemir, 1997, pp. 61-66), fairly enhancing the magnetization while cooling.

#### 4.4 X-ray fluorescence analysis

The intensity and magnitude of alterations in the magnetic mineralogy of basalt could be traced using various alteration indices (Nesbitt and Young, 1984; Nesbitt and Wilson, 1992; Fedo et al., 1995; Babechuk et al., 2014). The CIA values primarily track dissolution of feldspar and higher values promote the removal of labile elements (Ca, Na and K) (Babechuk et al., 2014). CIA greater than 99% indicates complete removal of mobile elements and retention of Aluminium (Fig. 7a) (Table 3, Supplementary file). CIA values for basalt are less than 33% which are well within the basaltic weathering range (Fig. 7a). In SAF triangular diagram, all laterite samples fall in moderately to strongly lateritised fields, suggesting the deep nature of weathering in a complete profile (Fig. 7b). In the laterites from Gujarat, Meshram & Randive (2011) reported similar strong lateritization from the SAF diagrams. The IOL is a prime index of lateritization whose values in these laterites are significantly higher (greater than 70%) (Fig. 7b). Basaltic sample at the base fall in kaolinitised field in SAF diagram (this could represent the initiation of lateritization process in *Zone III*) (Fig. 7b). The basalt IOL values are consistent with values obtained by Babechuk et al. (2014). Lastly, the MIA (oxidation) represents the retention of  $\text{Fe}^{3+}$  and aluminium over other oxides eventually noting the vital characteristics of laterite formation. As seen in Fig. 7c, all the laterite samples fall on the  $\text{Fe}_2\text{O}_3\text{-Al}_2\text{O}_3$  line indicating their enrichment and maturity.

Above mentioned alteration diagrams clearly indicate absolute maturation of the laterite profile and completion of the lateritization process. The conversion of magnetic minerals from basaltic lithology has experienced laterite weathering to the fullest possible extent. This strengthens our inference of detrital ferrimagnetic input in the highest horizons of laterites contributing to ferrimagnetism in an AFM dominant process of lateritization.

#### 4.5 X-ray diffraction analysis

The XRD analyses have been extensively practiced both quantitatively and qualitatively to study geological formations. We used *Match-3* software to analyse and refine the XRD data (<http://www.crystalimpact.com/match/>). This software utilizes extensive data library search to identify the mineral phases in the sample. We found background noise in the data similar to Suhr et al. (2018) which was later assigned to the widespread occurrence of ferrihydrite and amorphous phases of hematite. Iron and aluminium oxides and hydroxides along with clay minerals were observed throughout the laterite profile. Majority of the iron oxide and hydroxide peaks occur at  $30^\circ$  ( $2\theta$ ) onwards. Identification of maghemite and magnetite is challenging as their maximum peaks coincide. However, magnetite does not exhibit a peak at lower values of  $2\theta$  ( $25^\circ$ ). Stoichiometric hematite

produced characteristic peaks in the XRD spectra (Fig. 8). Furthermore, the Al-hematite peaks (d-values: 2.2076, 1.4552) are identified using software's library and the XRD spectra of Al-hematite in Roberts et al. (2006). The higher Al-substitution in hematite moves 2 thetas to higher values (Roberts et al., 2006). Furthermore, hematite and goethite peaks were checked and confirmed using XRD data of France and Oldfield (2000). XRD spectra of samples representing all the three zones are shown in Fig. 8. The minerals identified are gibbsite, Al-hematite, maghemite, goethite, hematite, ferrihydrite, and kaolinite (Fig. 8). Similar minerals were observed by Singh et al. (2020) while studying the laterites from the nearby Patan (Satara, Maharashtra) area of Deccan province. The XRD for basalt samples detected characteristic minerals of the rock (plagioclase, pyroxene, olivine, and minor quartz) (Fig. 8c). Initiation of the process of lateritization due to weathering of parent rock (formation of saprolite) could affect the primary mineral assemblage resulting in the formation of secondary clay minerals. Minor magnetic enhancement during thermomagnetic (high temperature) treatments is probably due to the conversion of these minerals into new magnetic mineral phases (e.g., magnetite; Jiang et al., 2015) (Fig. 6f).

The exact quantification of minerals by XRD spectra depends on crystal structure of the mineral phase present, their substitution, defects, polytypes, and also peak collisions (Zhou et al., 2018). Substitution and varying crystallinity are possible in laterites evident from their behaviour during thermomagnetic analysis. In this regard, laterite from *Zone I* and *Zone II* show similar mineralogy in XRD spectra but for their relative quantification, we rely on characteristic rock magnetic parameters because of earlier discussed factors.

The laterite mineralogy being complex, the results produce several uncertainties in XRD spectra. A dedicated study focussing on the mineralogical aspects of laterites using advanced microscopy (scanning electron microscopy) is required for the identification of the full spectrum of minerals (magnetic and non-magnetic). Therefore, maintaining the focus upon the main objectives of rock magnetism and palaeomagnetism, further spectroscopic analysis on mineral separates were restricted and the overall information based on XRD and rock magnetism endorsed the presence of at least two varieties of hematite (crystalline and amorphous), the goethite (with substitutions); maghemite, and possible products of partial maghemitization of magnetites. Rock magnetism also suggested a mixture of SD+SP+MD and SD+SP under dominant antiferromagnetic mineralogy. Thermomagnetic data confirmed the existence of goethite, maghemite, and magnetite. XRD showed kaolinite as a dominant clay mineral along with goethite, hematite, and gibbsite and their substitutional varieties.

## 4.6 NRM Acquisition

Above mineralogical studies infer that these laterites are enriched with both amorphous and crystalline antiferromagnetic oxides as the possible agents of NRM in the form of chemical/crystallization remanent magnetization (CRM). Amongst the two, crystalline hematites are the best possible candidates for stable and characteristic remanent magnetization (ChRM). On these premises, we conducted the palaeomagnetic analysis using alternating field demagnetization on the set of representative sister samples and are described below.

We relied upon the alternating field demagnetization, as thermal demagnetization was highly susceptible to laboratory heating-induced changes due to the abundance of amorphous and poorly crystalline iron oxide/hydroxide complexes (limonitic – ferrihydrites) and the presence of goethites resulting in strong secondary magnetization. The AF (alternating field) demagnetization on the other hand yielded convincing intensity decay as well as vector migration paths. The progressive demagnetization was carried up to the fields of 150 mT and showed stable components of remanence (Fig. 9).

We found sudden increase in magnetization at 5 mT (Fig. 9e) due to the removal of antiparallel or high angle viscous component, increasing the intensity for the resultant component. This followed a steady decay even at higher fields depicting single stable component in the NE direction. Alternating fields up to 150 mT removed large, low stability components parallel/subparallel to the NRM directed towards NE with an inclination of  $\sim 10^\circ$ . For majority of the samples, we found a trend in intensity decay partitioned into 0-25 mT and 60-150 mT. All the secondary components were removed by 25 mT depicting the ferrimagnetic components, further, there is a 90% loss of intensity by 150 mT (Fig. 9e).

The equal-area projection for the demagnetization spectra for specimen 2.1 shows a well-clustered nature with stable declination (D) and inclination (I) values. It shows the D/I values of  $10^\circ$  and  $46^\circ$ , respectively (Fig. 9a). Specimen 2.5 showed a sudden increase in intensity at the demagnetizing field of 5 mT, similar to the previous sample (Fig. 9f). Afterwards, there is complete decay or removal of remanent magnetization linearly from 5 to 25 mT. The equal-area projection shows good clustering of data with constant inclination and declination. Similar results were obtained for specimens 2.8 and 2.10. Specimens 3.1 and 3.5 showed a scattering of data in equal-area projection, although there is smooth decay in the fields of 0-25 mT and then 60-150 mT (not shown). These specimens show unimodal ChRM components without any secondary magnetization. Specimen 3.8

show stepwise decay of intensity of magnetization (Fig. 9g). Specimen 4.5 showed overlapping components with scattering in equal-area projection (Fig. 9d, 9h).

Further, in order to test the stability of NRM, we have calculated the Koenisberger ratio (Q-ratio) (Koenisberger, 1938) using the equation  $Q = \text{NRM (A/m)} / [\chi \text{ (SI)} \times H \text{ (A/m)}]$ , where  $\chi$  indicates the magnetic susceptibility and H represents the local geomagnetic field (Table 4, Supplementary file). The Q-ratio for present samples was calculated taking local geomagnetic field value of 34.18 A/m referred from International Geomagnetic Reference Field (12<sup>th</sup> Generation) values. The values  $Q > 1$  indicate remanent magnetization dominates over induced magnetization (Clark, 1997; Dunlop and Ozdemir, 1997, pp. 238-239) and the contribution of remanence properties is major to the total magnetization of the rock. Fig. 9i shows an upward rise in the Q-ratio along the laterite profile suggesting that the rock possesses stable carriers that can hold stable remanence.

The median destructive field (MDF) of NRM is the magnetic field required to eliminate half the remanent saturation magnetization (Dankers, 1981; Brachfeld and Banerjee, 2000). This parameter measures remanence stability by targeting the carriers of natural and induced remanences (Brachfeld and Banerjee, 2000). It is calculated by AF demagnetizing the sample through steps until we get the one-half value of the original NRM (Table 5, Supplementary file). MDF of studied samples increases upward in profile suggesting more stable remanence carriers (Fig. 9j). Generally, lower values of MDF of NRM suggest magnetite-titanomagnetite mineral phases while higher values suggest hematite-goethite minerals phases (Dankers, 1981).

The primary remanent magnetization (ChRM) in the studied samples was thus obtained after removal of the viscous components (at  $< 5$  mT), while the secondary remanence due to ferrimagnetic components are removed by 25 mT (Fig. 9). This indicates that the stable CRM in laterites is attributed to a sufficiently long duration of the process of lateritization surpassing the time of lock-in remanence. The amorphous AFMs appear to have little or no influence in disturbing or overprinting the NRM and can be demagnetized at low field values of 5 mT. The study, therefore, indicated: a) suitability of laterites to acquire stable NRMs and b) Crystalline hematite as benchmark mineral to record the NRM within the complex process of lateritization.

## **5. Basaltic Weathering and Natural Remanent Magnetization**

Basalts are some of the most susceptible substrates to chemical weathering under a large spectrum of Eh-pH and temperature conditions. The basaltic weathering is an effective process of CO<sub>2</sub> sequestration (Gislason and Oelkers, 2014), while it is considered a possible analogy to the Martian weathering conditions (Greenberger and Mustard, 2012) due to the existence of both basalt and

hematite over the planet. Another very important aspect of the basalts and their weathering products is its enrichment with ferrimagnetic minerals which can have unique pathways of conversions to maghemite and hematite. Lateritization permits sufficient reaction time and porosity for fluid migrations to convert these ferrimagnetic sources into antiferromagnetic, apart from the conversion of several other Fe oxides bearing silicates to such end product. Geologically laterites contribute to significant information on the paleogeographic status of a continent. The longitudinally drifting continent like India further preserve an important record of paleolatitudes to be determined from palaeomagnetic and magnetostratigraphic approaches.

Our studies have broadly inferred the total transformation of the parent basalts into antiferromagnetic during lateritization; and ferrimagnetism if any present is because of the lateral/surficial inputs during the process of lateritization. The abundance of feldspars in these basalts is also a possible reason for the early advancement of lateritization. The feldspar weathering has created labile elements besides their larger grain size providing effective porosity for the migration of solution. Early weathering of feldspar is also the source of ionic Al- to be readily available for substitution with ferrihydrites and hence hematites and goethite. The abundance of solution due to precipitations and humid conditions near the coast further accelerated the formation of limonites and goethite; which later permitted the formation of amorphous hematites by release of hydroxyl ions. Further maturity formed the crystalline hematites as the stable and advanced stage of lateritization reached. Once formed, the crystalline hematite (*hc*) remained stable preserving the NRM's. The process of formation of crystalline hematites (*hc*) from the amorphous hematites (*ha*) strengthened the CRM with sufficient time for lock-in, although a possibility of superimposition of CRMs cannot be ruled out. Our palaeomagnetic results could not trace such superimposition and almost a unimodal *hc* component was detected in these samples. However, a strong secondary component is observed due to ferrimagnetism (removed at 25 mT) which was accommodated as surficial input as discussed above.

This type of remanence acquired during the conversion of one mineral phase to another predominantly lead to growth-CRM (Haigh, 1958; Stokking and Tauxe, 1990) and can be strongly represented by primary remanence in palaeomagnetic studies (Walker et al., 1981). Hematites can be crystallized through various pathways, directly from the hydrolysis of ferric iron salts (Schwertmann and Cornell, 2000, pp. 121-134) or indirectly via the ferrihydrite → hematite reaction (Schwertmann and Cornell, 2000, pp. 121-134), later being common during the initial process of lateritization anticipating the strong CRM.

The CRM is acquired below their Curie/Neel points during the conversion of one mineral phase to another (Dekkers and Linssen, 1989; Jiang et al., 2015). CRM can be simple crystal growth (growth-



CRM) or the alteration of parent magnetic minerals (alteration-CRM) (Haigh, 1958; Stokking and Tauxe, 1990). In laterites, there are several possibilities for the unstable/transitional nature of the components. Such components can arise from; i) partial transformations of detrital magnetite to maghemite, ii) partial transformation of amorphous to crystalline hematites, iii) re-lateritization of the re-deposited or precipitated laterites, iv) post formation deformation within laterite zones imparting porosity, or v) groundwater-related activity in the porous laterite. The crystalline hematites are developed only during matured stage of lateritization, and they tend to remain stably prevented from the secondary magnetization, although the deformation may cause physical scattering of directions. Alternatively, the CRM in these laterites arises from crystallization remanent magnetization (*sensu stricto*). Our study depicted the middle zone to be more mature and abundant with SD hematites, whereas the upper zone is influenced by surficial ferruginous/lateritic inputs. The CRMs therefore can be used reliably for the magnetostratigraphic approach in the Deccan laterites, when the surficial inputs, deformation, and other disturbances are restricted. The present approach of palaeomagnetism combined with mineral magnetism can be developed to understand the otherwise complex nature of timing in the lateritic processes. Determination of the timing of degree of lateritization at various stages is therefore helpful in studying various applications including CO<sub>2</sub> sequestration and Martian weathering analogy.

## 6. Conclusions

The Deccan Laterites represent peak basaltic weathering conditions by complete ferri- to antiferromagnetic transformations and further mobilizations within antiferromagnetic oxides. The combination of rock magnetism, XRD spectroscopy, palaeomagnetism, and XRF analysis provide an ideal approach to characterize the mineralogical influence over natural remanence. This integrated study inferred a set of minerals depicting partial to complete maghemitization, total hematization, goethite formation, ferrihydrite complexes, and their Al-substituted varieties in addition to gibbsite and kaolinite. The abundance of amorphous- (*ha*) and crystalline hematite (*hc*) varieties interests the palaeomagnetic studies to investigate the nature of NRMs, while the ferrimagnets are represented as secondary components. A range of domain sizes occurs with mixtures of SP+SD and SP+SD+MD, and SD remains common to most of the profile. The secondary/viscous NRM due to *ha* is removed at 5 mT and the secondary component due to ferrimagnets (magnetite or maghemites) removed at 25 mT. The *hc* component continues to decay linearly up to 150 mT depicting unicomponent behaviour after 25 mT. The palaeomagnetic tests (Koenisberger ratio, MDF, intensity decay, and Zijderveld diagrams) indicated stable directions (ChRMs) due to *hc*; and the Al-substitution does not affect the stability of ChRM. The lock-in CRM from *hc* also benchmarks the maturity of the profile in terms of mineralogical

advancement during lateritization. These laterites are thus ideal for palaeomagnetic studies and intricacies and scattered directions may arise from other secondary processes during lateritization such as internal deformation and solution/precipitation activities through secondary porosity. The ferrimagnetic abundance in basaltic laterites permits a large amount of crystalline hematite which once formed remain stable favouring reliable ChRM directions due to CRM.

### **Acknowledgments**

We greatly acknowledge the anonymous referees and the handling editors for many critical comments and suggestions that improved the previous version of this manuscript. Several limitations and uncertainties in the XRD results were identified by anonymous referee, is acknowledged. We acknowledge Head, Department of Geology, Savitribai Phule Pune University for encouragement and support; Ministry of Earth Science grant MoES/P.O. (Seismo)/1(353)/2018-2019 funding for analysis. Director, CSIR-National Geophysical Research Institute (Hyderabad) and Director, CSIR-National Institute of Oceanography (Goa) are acknowledged for encouragements, support and permissions during analyses.

### **References**

- Babechuk, M., Widdowson, M., Kamber, B., 2014. Quantifying chemical weathering intensity and trace element release from two contrasting basalt profiles, Deccan Traps, India. *Chem. Geol.* 363, 56-75. <https://doi.org/10.1016/j.chemgeo.2013.10.027>
- Babechuk, M., Widdowson, M., Murphy, M., Kamber, B., 2015. A combined Y/Ho, high field strength element (HFSE) and Nd isotope perspective on basalt weathering, Deccan Traps, India. *Chem. Geol.* 396, 25-41. <https://doi.org/10.1016/j.chemgeo.2014.12.017>
- Bardossy, G., 1981. Paleoenvironments of laterites and lateritic bauxites – effect of global tectonism on bauxite formation. In: *International Seminar on Lateritization Processes* (Trivandrum, India), Rotterdam, Balkema, pp. 284-297.
- Borger, H., Widdowson, M., 2001. Indian laterites, and lateritous residues of southern Germany: a petrographic, mineralogical, and geochemical comparison. *Zeit. Für Geomorph. N.F.* 45, 177-200. <https://doi.org/10.1127/zfg/45/2001/177>
- Bourman, R., Ollier, C., 2002. A critique of the Schellmann definition and classification of ‘laterite’. *Catena* 47 (2), 117-131. [https://doi.org/10.1016/S0341-8162\(01\)00178-3](https://doi.org/10.1016/S0341-8162(01)00178-3)
- Brachfeld, S.A., Banerjee, S.K., 2000. A new high-resolution geomagnetic relative paleointensity record for the North American Holocene: A comparison of sedimentary and absolute intensity data. *J. Geophys. Res. Solid Earth* 105 (B1), 821-834. <https://doi.org/10.1029/1999JB900365>
- Buchanan, F., 1807. *A Journey from Madras through the Countries of Mysore, Kanara, and Malabar* 2 & 3. London, East India Company.

- Caner, L., Petit, S., Joussein, E., Fritsch, E., Herbillon, A., 2011. Accumulation of organo-metallic complexes in laterites and the formation of Aluandic Andosols in the Nilgiri Hills (southern India): similarities and differences with Umbric Podzols. *Europ. J. Soil. Sci.* 62 (5), 754-764. <https://doi.org/10.1111/j.1365-2389.2011.01389.x>
- Clark, D.A., 1997. Magnetic petrophysics and magnetic petrography: aids to geological interpretation of magnetic surveys. *AGSO J. Aust. Geol. Geophys.* 17, 83-103.
- Cornell, R.M., Schwertmann, U., 2003. The iron oxides: structure, properties, reactions, occurrence and uses. Wiley-VCH Verlag GmbH & Co. KGaA, Weinheim.
- Courtillot, V., Feraud, G., Maluski, H., Vandamme, D., Moreau, M.G., Besse, J., 1988. Deccan flood basalts and the Cretaceous Tertiary boundary. *Nature* 333, 843-846. <https://doi.org/10.1038/333843a0>
- Dankers, P., 1981. Relationship between median destructive field and remanent coercive forces for dispersed natural magnetite, titanomagnetite and hematite. *Geophys. J. Royal Astron. Soc.* 64, 447-461. <https://doi.org/10.1111/j.1365-246X.1981.tb02676.x>
- Day, R., Fuller, M., Schmidt, V.A., 1977. Hysteresis properties of titanomagnetites: Grain size and composition dependence. *Phys. Earth Plan. Int.* 13, 260-267. [https://doi.org/10.1016/0031-9201\(77\)90108-X](https://doi.org/10.1016/0031-9201(77)90108-X)
- Dekkers, M.J., 1988. Magnetic behaviour of natural goethite during thermal demagnetization. *Geophys. Res. Lett.* 15 (5), 538-541. <https://doi.org/10.1029/GL015i005p00538>
- Dekkers, M.J., 1990. Magnetic properties of natural goethite-III. Magnetic behaviour and properties of minerals originating from goethite dehydration during thermal demagnetization. *Geophys. J. Int.* 103, 233-250. <https://doi.org/10.1111/j.1365-246X.1990.tb01765.x>
- Dekkers, M.J., Linssen, J.H., 1989. Rock magnetic properties of fine-grained natural low temperature haematite with reference to remanence acquisition mechanisms in red beds. *Geophys. J. Int.* 99, 1-18. <https://doi.org/10.1111/j.1365-246X.1989.tb02012.x>
- Dekkers, M.J., Rochette, P., 1992. Magnetic properties of chemical magnetisation in synthetic and natural goethite: prospects for a natural remanent magnetisation/thermoremanent magnetisation ratio paleomagnetic stability test?. *J. Geophys. Res. Solid Earth* 97, 17291-17307. <https://doi.org/10.1029/92JB01026>
- Dunlop, D.J., 2002. Theory and application of the Day plot (Mrs/Ms versus Hcr/Hc), 1. Theoretical curves and tests using titanomagnetite data. *J. Geophys. Res. Solid Earth* 107 (B3), EPM 4-1-EPM 4-22. <https://doi.org/10.1029/2001JB000486>
- Dunlop, D.J., Özdemir, Ö., 1997. *Rock Magnetism, Fundamentals and Frontiers*. Cambridge University Press, Cambridge, U. K. <https://doi.org/10.1017/CBO9780511612794>
- Duraiswami, R.A., Gadpallu, P., Shaikh, T.N., Cardin, N., 2014. Pahoehoe-a'a transitions in the lava flow fields of the western Deccan Traps, India-implications for emplacement dynamics, flood basalt architecture and volcanic stratigraphy. *J. Asian Earth Sci.* 84, 146-166. <https://doi.org/10.1016/j.jseas.2013.08.025>

- Egli, R., Lowrie, W., 2002. Anhysteretic remanent magnetization of fine magnetic particles. *J. Geophys. Res. Solid Earth* 107 (B10), 2209. <https://doi.org/10.1029/2001JB000671>
- Evans, M.E., Heller, F., 2003. *Environmental magnetism: principles and applications of enviromagnetics*. Academic press, San Diego, California.
- Farmer, V.C., 1974. *The Infrared Spectra of Minerals*. Cambridge University Press, Cambridge. <https://doi.org/10.1180/mono-4>
- Fedo, C., Nesbitt, H., Young, G., 1995. Unraveling the effects of potassium metasomatism in sedimentary rocks and paleosols, with implications for paleoweathering conditions and provenance. *Geology* 23, 921-924. [https://doi.org/10.1130/0091-7613\(1995\)023<0921:UTEOPM>2.3.CO;2](https://doi.org/10.1130/0091-7613(1995)023<0921:UTEOPM>2.3.CO;2)
- France, D.E., Oldfield, F., 2000. Identifying goethite and hematite from rock magnetic measurements of soils and sediments. *J. Geophys. Res. Solid Earth* 105, 2781-2795. <https://doi.org/10.1029/1999JB900304>
- Ghosh, S., Guchhait, S.K., Hu, X., 2015. Characterization and evolution of primary and secondary laterites in northwestern Bengal Basin, West Bengal, India. *J. Paleogeography* 4 (2), 203-230. <https://doi.org/10.3724/SP.J.1261.2015.00074>
- Gislason, S.R., Oelkers, E.H., 2014. Carbon storage in basalt. *Science*. 344 (6182), 373-374. <https://doi.org/10.1126/science.1250828>
- Greenberger, R.N., Mustard, J.F., Kumar, P.S., Dyar, M.D., Breves, E.A., Sklute, E.C., 2012. Low temperature aqueous alteration of basalt: Mineral assemblages of Deccan basalts and implications for Mars. *J. Geophys. Res. Planets*. 117, E00J12. <https://doi.org/10.1029/2012JE004127>
- Gunnell, Y., 2003. Radiometric ages of laterites and constraints on long-term denudation rates in West Africa. *Geology* 31 (2), 131. [https://doi.org/10.1130/0091-7613\(2003\)031<0131:RAOLAC>2.0.CO;2](https://doi.org/10.1130/0091-7613(2003)031<0131:RAOLAC>2.0.CO;2)
- Haigh, G., 1958. The process of magnetization by chemical change. *Phil. Mag.* 3, 267-286. <https://doi.org/10.1080/14786435808238219>
- Heslop, D., 2009. On the statistical analysis of the rock magnetic S-ratio. *Geophys. J. Int.* 178 (1), 159–161. <https://doi.org/10.1111/j.1365-246X.2009.04175.x>
- Heslop, D., Dekkers, M.J., Kruiver, P.P., Van Oorschot, I.H.M., 2002. Analysis of isothermal remanent magnetisation acquisition curves using the expectation-maximisation algorithm. *Geophys. J. Int.* 148, 58-64. <https://doi.org/10.1046/j.0956-540x.2001.01558.x>
- Hu, P., Jiang, Z., Liu, Q., Heslop, D., Roberts, A.P., Torrent, J., Barrón, V., 2016. Estimating the concentration of aluminum-substituted hematite and goethite using diffuse reflectance spectrometry and rock magnetism: Feasibility and limitations. *J. Geophys. Res. Solid Earth*. 121, 4180-4194. <https://doi.org/10.1002/2015JB012635>
- Hynek, B.M., Arvidson, R.E., Phillips, R.J., 2002. Geologic setting and origin of Terra Meridiani hematite deposit on Mars. *J. Geophys. Res. Solid Earth* 107 (E10), 5088. <https://doi.org/10.1029/2002JE001891>

- Jiang, Z., Liu, Q., Roberts, A.P., Dekkers, M.J., Barrón, V., Torrent, J., Li, S., 2022. The magnetic and color reflectance properties of hematite: From Earth to Mars. *Reviews of Geophysics* 60 (1), e2020RG000698. <https://doi.org/10.1029/2020RG000698>
- Jiang, Z., Liu, Q., Zhao, X., Jin, C., Liu, C., Li, S., 2015. Thermal magnetic behaviour of Al-substituted haematite mixed with clay minerals and its geological significance. *Geophys. J. Int.* 200, 130-143. <https://doi.org/10.1093/gji/ggu377>
- King, J., Channell, J.E., 1991. Sedimentary magnetism, environmental magnetism, and magnetostratigraphy. *Rev. Geophys.* 29, 358-370. <https://doi.org/10.1002/rog.1991.29.s1.358>
- Kısakürek, B., Widdowson, M., James, R., 2004. Behaviour of Li isotopes during continental weathering: The Bidar laterite profile, India. *Chem. Geol.* 212, 27-44. <https://doi.org/10.1016/j.chemgeo.2004.08.027>
- Kletetschka, G., Wasilewski, P.J., 2002. Grain size limit for SD hematite. *Phys. Earth Planet. Int.* 129 (1-2), 173-179. [https://doi.org/10.1016/S0031-9201\(01\)00271-0](https://doi.org/10.1016/S0031-9201(01)00271-0)
- Klootwijk, C.T., Pierce, J.W., 1979. India's and Australia's pole path since the late Mesozoic and the India-Asia collision. *Nature* 282, 605-607. <https://doi.org/10.1038/282605a0>
- Koenigsberger, J.G., 1938. Natural residual magnetism of eruptive rocks. *Terr. Magn. Atmos. Electr.* 43 (3), 299-320. <https://doi.org/10.1029/TE043i003p00299>
- Kruiver, P.P., Dekkers, M.J., Heslop, D., 2001. Quantification of magnetic coercivity components by the analysis of acquisition curves of isothermal remanent magnetization. *Earth Planet. Sci. Lett.* 189, 269-276. [https://doi.org/10.1016/S0012-821X\(01\)00367-3](https://doi.org/10.1016/S0012-821X(01)00367-3)
- LaBrecque, J.J., Schorin, H., 1987. Some statistical parameters for selected trace elements in VL-1. *Z. Geomorphol. N.F.* 64, 33-38.
- Landis, G.A., Blaney, D., Cabrol, N., Clark, B.C., Farmer, J., Grotzinger, J., Geeley, R., McLennan, S.M., Richter, L., Yen, A., The Mer Athena Science Team, 2004. Transient liquid water as a mechanism for induration of soil crusts on Mars. *Lunar and Planetary Science Conference XXXV*, Abstract 2188.
- Liu, Q. S., Deng, C.L., Yu, Y.J., Torrent, J., Jackson, M.J., Banerjee, S.K., Zhu, R.X., 2005. Temperature dependence of magnetic susceptibility in an argon environment: Implications for pedogenesis of Chinese loess/palaeosols. *Geophys. J. Int.* 161, 102-112. <https://doi.org/10.1111/j.1365-246X.2005.02564.x>
- Liu, Q., Jackson, M. J., Banerjee, S. K., Maher, B. A., Deng, C., Pan, Y., Zhu, R., 2004. Mechanism of the magnetic susceptibility enhancements of the Chinese loess. *J. Geophys. Res. Solid Earth* 109, B12107. <https://doi.org/10.1029/2004JB003249>
- Liu, Q., Roberts, A.P., Larrasoña, J.C., Banerjee, S.K., Guyodo, Y., Tauxe, L., Oldfield, F., 2012. Environmental magnetism: Principles and applications. *Rev. Geophys.* 50, RG4002. <https://doi.org/10.1029/2012RG000393>
- Liu, Q., Roberts, A.P., Torrent, J., Horng, C.S., Larrasoana, J.C., 2007. What do the HIRM and S-ratio really measure in environmental magnetism?. *Geochem. Geophys. Geosyst.* 8, Q09011. <https://doi.org/10.1029/2007GC001717>

- Liu, X., Mao, X., Yuan, Y., Ma, M. 2019. Aeolian accumulation: An alternative origin of laterite on the Deccan Plateau, India. *Paleogeogr., Paleoclim., Paleoeco.* 518, 34-44. <https://doi.org/10.1016/j.palaeo.2019.01.003>
- Maher, B.A., 1988. Magnetic properties of some synthetic submicron magnetites. *Geophys. J. Int.* 94, 83–96. <https://doi.org/10.1111/j.1365-246X.1988.tb03429.x>
- Maher, B.A., Thompson, R., 1999. *Quaternary climates, environments and magnetism.* Cambridge university press, New York.
- Maxbauer, D.P., Feinberg, J.M., Fox, D.L., 2016. MAX UnMix: A web application for unmixing magnetic coercivity distributions. *Comp. Geosc.* 95, 140-145. <https://doi.org/10.1016/j.cageo.2016.07.009>
- Meshram, R., Randive, K., 2011. Geochemical study of laterites of the Jamnagar district, Gujarat, India: Implications on parent rock, mineralogy and tectonics. *J. Asian Earth Sci.* 42, 1271-1287. <https://doi.org/10.1016/j.jseaes.2011.07.014>
- Nesbitt, H.W., Wilson, R.E., 1992. Recent chemical weathering of basalts. *Am. J. Sci.* 292, 740-777. [10.2475/ajs.292.10.740](https://doi.org/10.2475/ajs.292.10.740)
- Nesbitt, H.W., Young, G.M., 1984. Prediction of some weathering trends of plutonic and volcanic rocks based on thermodynamic and kinetic considerations. *Geoch. Cosmoch. Acta.* 48 (7), 1523-1534. [https://doi.org/10.1016/0016-7037\(84\)90408-3](https://doi.org/10.1016/0016-7037(84)90408-3)
- O'Reilly, W., 1984. *Rock and Mineral Magnetism.* Chapman and Hall, New York.
- Ollier, C.D., Sheth, H., 2008. The High Deccan duricrusts of India and their significance for the 'laterite' issue. *J. Earth Syst. Sci.* 117 (5), 537-551. <https://doi.org/10.1007/s12040-008-0051-9>
- Peters, C. and Dekkers, M.J., 2003. Selected room temperature magnetic parameters as a function of mineralogy, concentration and grain size. *Phys. Chem. Earth, Parts A/B/C* 28(16-19), 659-667. [https://doi.org/10.1016/S1474-7065\(03\)00120-7](https://doi.org/10.1016/S1474-7065(03)00120-7)
- Roberts, A. P., Liu, Q., Rowan, C.J., Chang, L., Carvallo, C., Torrent, J., Horng, C.S., 2006. Characterization of hematite ( $\alpha$ -Fe<sub>2</sub>O<sub>3</sub>), goethite ( $\alpha$ -FeOOH), greigite (Fe<sub>3</sub>S<sub>4</sub>), and pyrrhotite (Fe<sub>7</sub>S<sub>8</sub>) using first-order reversal curve diagrams. *J. Geophys. Res. Solid Earth* 111, B12S35. <https://doi.org/10.1029/2006JB004715>
- Roberts, A.P., Zhao, X., Heslop, D., Abrajevitch, A., Chen, Y.H., Hu, P., Jiang, Z., Liu, Q., Pillans, B.J., 2020. Hematite ( $\alpha$ -Fe<sub>2</sub>O<sub>3</sub>) quantification in sedimentary magnetism: limitations of existing proxies and ways forward. *Geosci. Lett.* 7 (1), 1-11. <https://doi.org/10.1186/s40562-020-00157-5>
- Robinson, S.G., 1986. The Late Pleistocene palaeoclimatic record of North Atlantic deep-sea sediments revealed by mineral magnetic measurements. *Phys. Earth Planet. Inter.* 42, 22-47. [https://doi.org/10.1016/S0031-9201\(86\)80006-1](https://doi.org/10.1016/S0031-9201(86)80006-1)
- Rochette, P., Mathe, P.E., Esteban, L., Rakoto, H., Bouchez, J.L., Liu, Q.S., Torrent, J., 2005. Non-saturation of the defect moment of goethite and fine-grained hematite up to 57 Teslas. *Geophys. Res. Lett.* 32, L22309. <https://doi.org/10.1029/2005GL024196>

- Sangode, S.J., Bloemendal, J., 2004. Pedogenic transformation of magnetic minerals in Pliocene-Pleistocene palaeosols of the Siwalik Group, NW Himalaya, India. *Palaeogeogr., Palaeoclim., Palaeoeco.* 212 (1-2), 95-118. <https://doi.org/10.1016/j.palaeo.2004.05.019>
- Schellmann, W., 1986. A new definition of laterite. In: Banerji, P.K. (Eds.), *Lateritisation processes*, Memoir of Geological Survey of India, pp. 1-7.
- Schmidt, P.W., Prasad, V., Raman, P.K., 1983. Magnetic ages of some Indian laterites. *Paleogeogr., Paleoclim., Paleoeco.* 44, 185-202. [https://doi.org/10.1016/0031-0182\(83\)90102-5](https://doi.org/10.1016/0031-0182(83)90102-5)
- Schuiling, R.D., Krijgsman, P., 2006. Enhanced weathering: an effective and cheap tool to sequester CO<sub>2</sub>. *Clim. Chang.* 74, 349-354. <https://doi.org/10.1007/s10584-005-3485-y>
- Schwertmann, U., Cornell, R.M., 2000. *Iron oxides in the laboratory*. Wiley-VCH Verlag GmbH, Weinheim. <https://doi.org/10.1002/9783527613229>
- Seifritz, W., 1990. CO<sub>2</sub> disposal by means of silicates. *Nature* 345, 486. <https://doi.org/10.1038/345486b0>
- Singh, J., Sangode, S.J., Bagwan, M.F., Meshram, D.C., Dhobale, A., 2020. Episodic ferricretization of the Deccan laterites (India): Inferences from ore microscopy, mineral magnetic and XRD spectroscopic studies. *J. Earth Syst. Sci.* 129, 76. <https://doi.org/10.1007/s12040-019-1334-z>
- Stokking, L.B., Tauxe, L., 1990. Properties of chemical remanence in synthetic hematite: Testing theoretical predictions. *J. Geophys. Res. Solid Earth* 95 (B8), 12639-12652. <https://doi.org/10.1029/JB095iB08p12639>
- Suhr, N., Schoenberg, R., Chew, D., Rosca, C., Widdowson, M., Kamber, B., 2018. Elemental and isotopic behaviour of Zn in Deccan basalt weathering profiles: Chemical weathering from bedrock to laterite and links to Zn deficiency in tropical soils. *Sci. Total Environ.* 619–620, 1451-1463. <https://doi.org/10.1016/j.scitotenv.2017.11.112>
- Tauxe, L., 2002. *Paleomagnetic principles and practice*. Kluwer academic press, London. <https://doi.org/10.1007/0-306-48128-6>
- Tauxe, L., Mullender, T.A.T., Pick, T., 1996. Potbellies, wasp-waists, and superparamagnetism in magnetic hysteresis. *J. Geophys. Res. Solid Earth* 101 (B1), 571-583. <https://doi.org/10.1029/95JB03041>
- Thomas, M., Clarke, J.D.A., Pain, C.F., 2005. Weathering, erosion and landscape processes on Mars identified from recent rover imagery, and possible Earth analogues. *Austr. J. Earth Sci.* 52 (3), 365-378. <https://doi.org/10.1080/08120090500134597>
- Thompson, R., Oldfield, F., 1986. *Environmental magnetism*, Allen and Unwin Press, London. <https://doi.org/10.1007/978-94-011-8036-8>
- Torrent, J., Barrón, V., Liu, Q., 2006. Magnetic enhancement is linked to and precedes hematite formation in aerobic soil. *Geophys. Res. Lett.* 33, L02401. <https://doi.org/10.1029/2005GL024818>.

- Walker, T.R., Larson, E.E., Hoblitt, R.P., 1981. Nature and origin of hematite in the Moenkopi Formation (Triassic), Colorado Plateau: A contribution to the origin of magnetism in red beds. *J. Geophys. Res. Solid Earth* 86(B1), 317-333. <https://doi.org/10.1029/JB086iB01p00317>
- Widdowson, M., 2007. Laterite and ferricrete. In: Nash, D.J., McLaren, S.J. (Eds.), *Geochemical Sediments and Landscapes*, Wiley-Blackwell, Oxford, UK, pp. 46-94.
- Widdowson, M., Cox, K.G., 1996. Uplift and erosional history of the Deccan Traps, India: Evidence from laterites and drainage patterns of the Western Ghats and Konkan Coast. *Earth Planet. Sci. Lett.* 137, 57-69. [https://doi.org/10.1016/0012-821X\(95\)00211-T](https://doi.org/10.1016/0012-821X(95)00211-T)
- Widdowson, M., Gunnell, Y., 1999. Lateritization, geomorphology and geodynamics of a passive continental margin: the Konkan and Kanara coastal lowlands of western Peninsula India. In: Thiry, M., Simon-Coinçon, R. (Eds.), *Palaeoweathering, Palaeosurfaces and Related Continental Deposits*, International Association of Sedimentologists, Oxford, Blackwell, pp. 245-274.
- Wimpenny, J.B., Gannoun, A., Burton, K.W., Widdowson, M., James, R.H., Gislason, S., 2007. Rhenium and osmium isotope and elemental behaviour accompanying laterite formation in the Deccan region of India. *Earth Planet. Sci. Lett.* 261 (1-2), 239-258. <https://doi.org/10.1016/j.epsl.2007.06.028>
- Zhang, C., Liu, Q., Huang, B., Su, Y., 2010. Magnetic enhancement upon heating of environmentally polluted samples containing haematite and iron. *Geophys. J. Int.* 181 (3), 1381-1394. <https://doi.org/10.1111/j.1365-246X.2010.04590.x>
- Zhou, X., Liu, D., Bu, H., Deng, L., Liu, H., Yuan, P., Du, P., Song, H., 2018. XRD-based quantitative analysis of clay minerals using reference intensity ratios, mineral intensity factors, Rietveld, and full pattern summation methods: A critical review. *Solid Earth Sci.* 3 (1), 16-29. <https://doi.org/10.1016/j.sesci.2017.12.002>
- Zijderveld, J., 1967. AC Demagnetization of rocks: Analysis of results. In: Collinson, D., Creer, K., Runcorn, S. (Eds.), *Methods in Paleomagnetism*, Elsevier, New York, pp. 254-286.



## Figure captions

**Figure 1.** Location map of the study area. a) High level (dark brown) and low level (orange) laterites separated by the Western Ghats escarpment (dashed red line). Black dot lines represent the elevation contours in meters. Inland water bodies are marked in blue colour. The study area (near Chiplun) is indicated by a black star. b) Geological map of the study area after Widdowson and Cox (1996). The Deccan trap stratigraphy is shown by shades of green colour. The studied laterites are developed on basalts belonging to Poladpur Formation of Deccan volcanic province (modified after Widdowson and Cox (1996)).

**Figure 2.** Bar plots of different environmental magnetic parameters against the specimens of their respective samples. Green-coloured bars represent Sample 1 (specimens 1A, 1B, 1C) of laterite and Sample 7 (specimens 7A, 7B, 7C, 7D) of basalt, while Sample 2-6 of the typical laterites are shown in red bars. Index on the lower right side of the diagram represents zones and their corresponding specimens. The parameters employed in this study are a)  $\chi_{lf}$  ( $10^{-8}$  m<sup>3</sup>/kg), b)  $\chi_{fd}$  %, c)  $\chi_{ARM}$  ( $10^{-6}$  m<sup>3</sup>/kg), d) SIRM (Am<sup>2</sup>/kg), e) S-ratio, f) SIRM/ $\chi$  ( $10^8$  A/m), g)  $\chi_{ARM}/\chi_{lf}$ , h) HIRM (Am<sup>2</sup>/kg), i)  $B_{cr}$  (mT), j) Soft IRM (Am<sup>2</sup>/kg), k) L-ratio.

**Figure 3.** The first row shows IRM acquisition (magnetization against applied field) for a sample from *Zone I*, *Zone II*, and *Zone III* in sequence. The second-row plots the coercivity spectra [ $d(M)/d(\log B)$ ] vs  $\log B$  mT for specimens from *Zone I* (d), and *Zone II* (e, f). The dashed lines represent the mean coercivity values of the components. In the third row, we have plotted the RPM (relative percentage of magnetization acquisition) for specimens belonging to *Zone I* (g) and *Zone II* (h, i). Letters A to O on the x-axis represents the intervals of applied field in mT. Acquisition steps are shown at the bottom of the figure.

**Figure 4.** Hysteresis curves for samples representing all three zones (*Zone-I*, *II* and *III*) from the studied profile. The figure shows wasp-waisted curves for laterite samples (b-e). The hysteresis curve of Sample 1 (laterite) showed similarity with the Sample 7 (basalt) (a, f).

**Figure 5.** Day-Dunlop plot (Day 1977; Dunlop, 2002). Domain state mixing lines are adopted from Dunlop (2002). Red circles indicate laterite samples (Sample 1-6) while green circle indicate basalt sample (Sample 7).

**Figure 6.** Thermomagnetic curves for laterites (Sample 1-5) and basalt (Sample 7). Distinct patterns of heating are observed for samples from *Zone I* (a), *Zone II* (b-e) and *Zone III* (f). Laterite samples showed large differences in the magnetization after heating and cooling cycles (irreversible behaviour). Reversible curves were produced for basaltic sample (Sample 7). Red and blue arrows indicate heating and cooling curves.

**Figure 7.** Ternary diagrams indicating changes in various oxides along with weathering indices. Laterites are marked by red circles while basalt samples are shown by green triangles. The first diagram (a) is A-CN-K ternary plot along with the chemical index of alteration (CIA) (Nesbitt and Young, 1984; Nesbitt and Wilson, 1992; Fedo et al., 1995). The second diagram (b) is S-A-F ternary plot after Schellmann (1986) indicating the degree of lateritization. A-L-F ternary plot (c) indicating losses of mafic against alkali oxides (Babechuk et al., 2014).

**Figure 8.** XRD diffraction patterns of samples representing all three zones. a) Sample 1 (Zone-I) b) Sample 3 (Zone-II) c) Sample 7 (Zone-III). The characteristic minerals identified are marked by numbers for laterite (sample 3) and small letters for basalt (sample 7). The d-values for the identified peaks are shown in blue coloured text. 1-Gibbsite, 2-Al-hematite, 3-Goethite, 4-Maghemite, 5-Hematite, 6-Kaolinite, a-Plagioclase, b-Pyroxene, c-Olivine, d-Quartz, e-Magnetite.

**Figure 9.** The equal area projection of vector migration (a, d, c, d) and the Zijderveld diagrams (e, f, g, h; Zijderveld, 1967) for representative laterite specimens. The nature of magnetic intensity decay curve for respective specimens is shown in the inset graphs. Variation in the Koenisberger ratio (Q-ratio) (i) indicating an upward increase along with the profile. The graph between sample numbers and median destructive field of NRM indicates an upward increase in MDF along with the laterite profile (j).

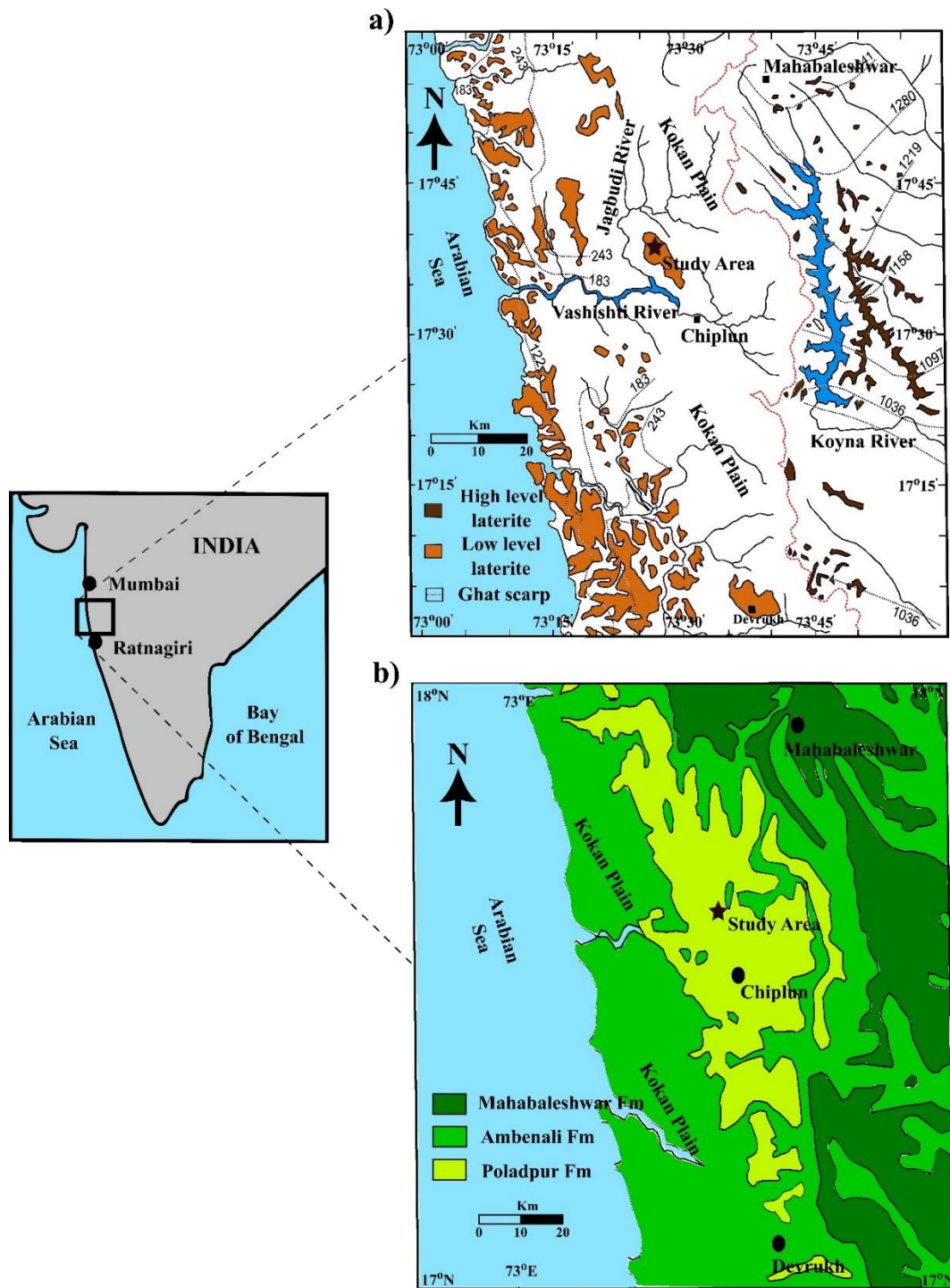


Figure 1

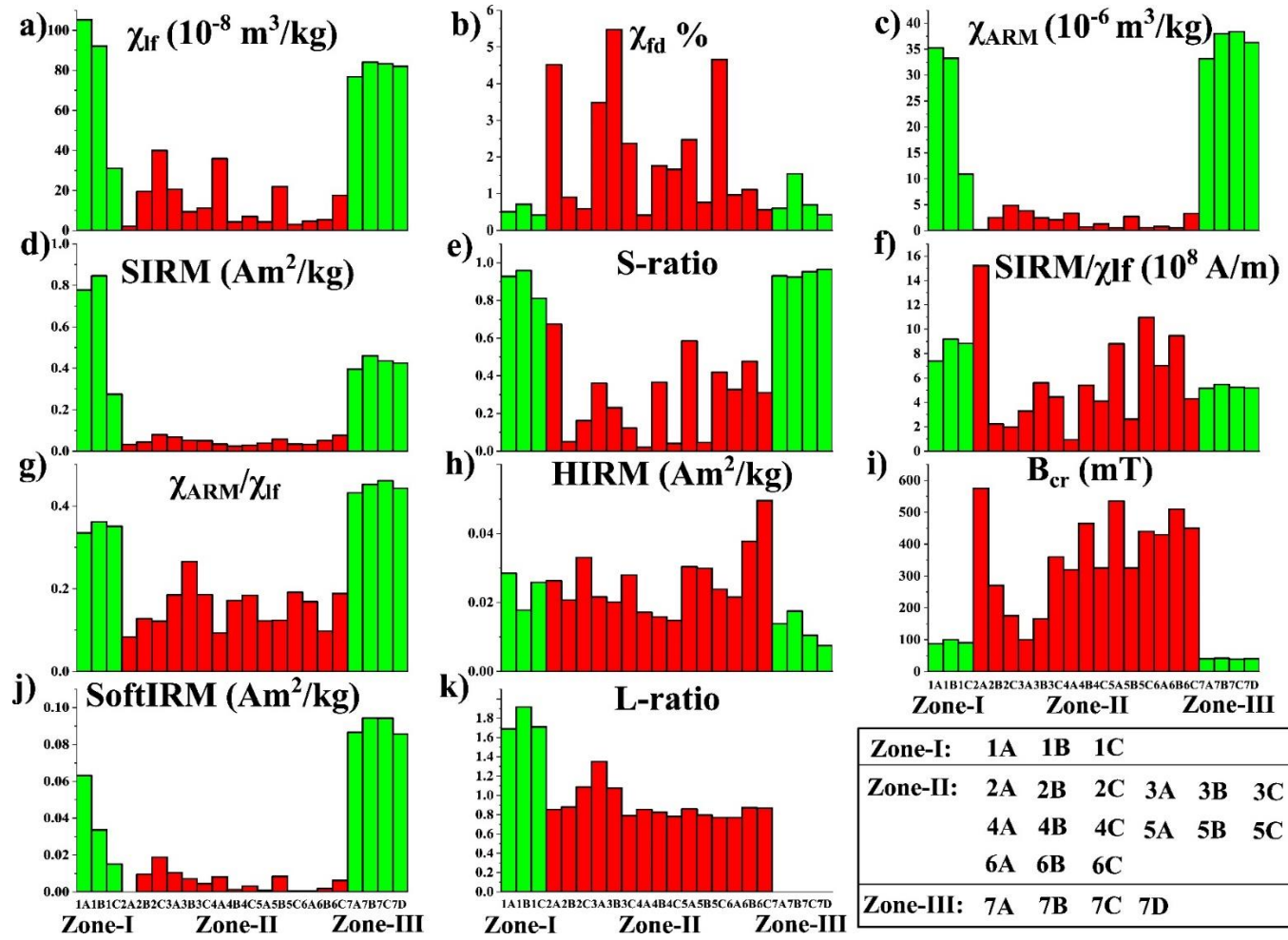


Figure 2

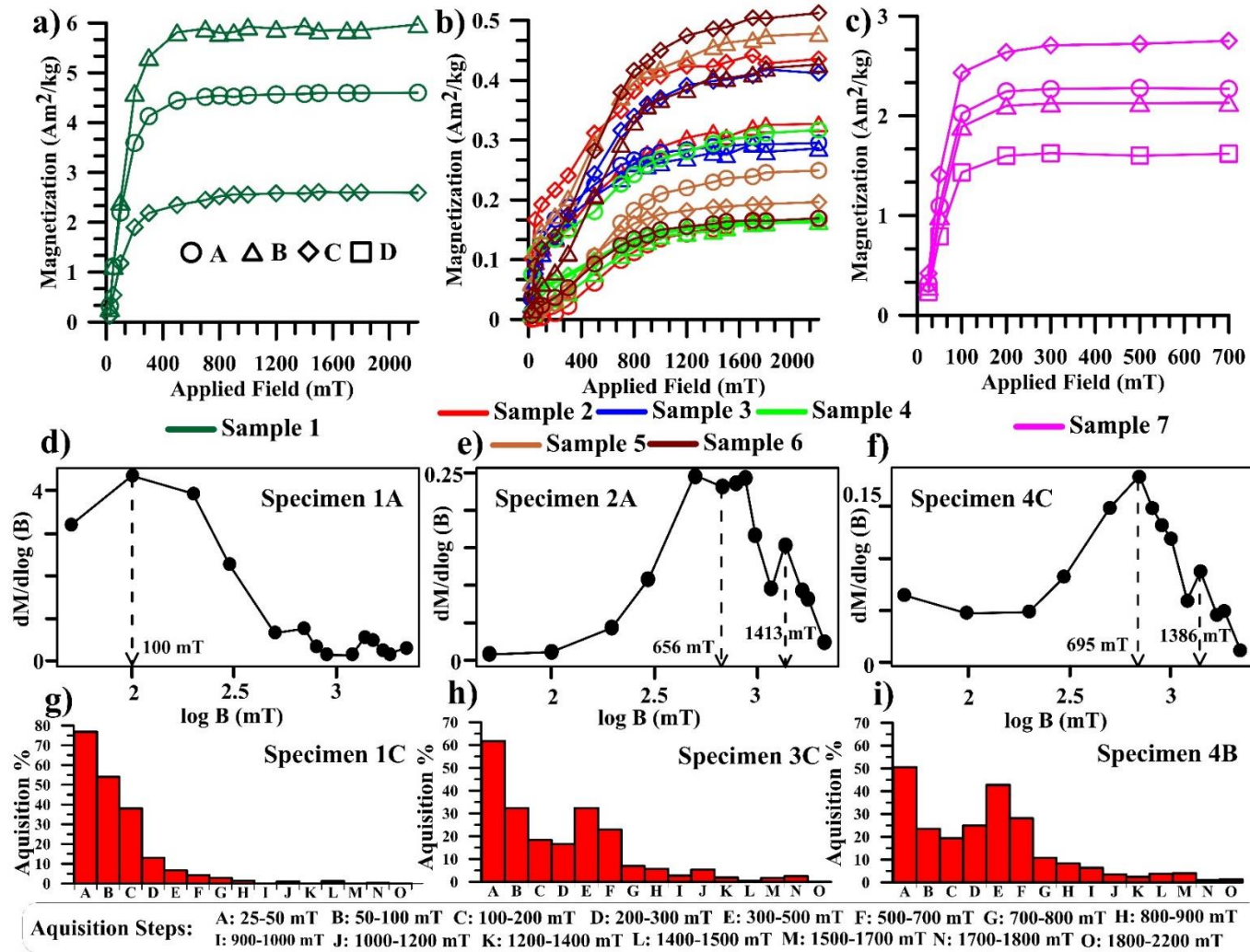


Figure 3

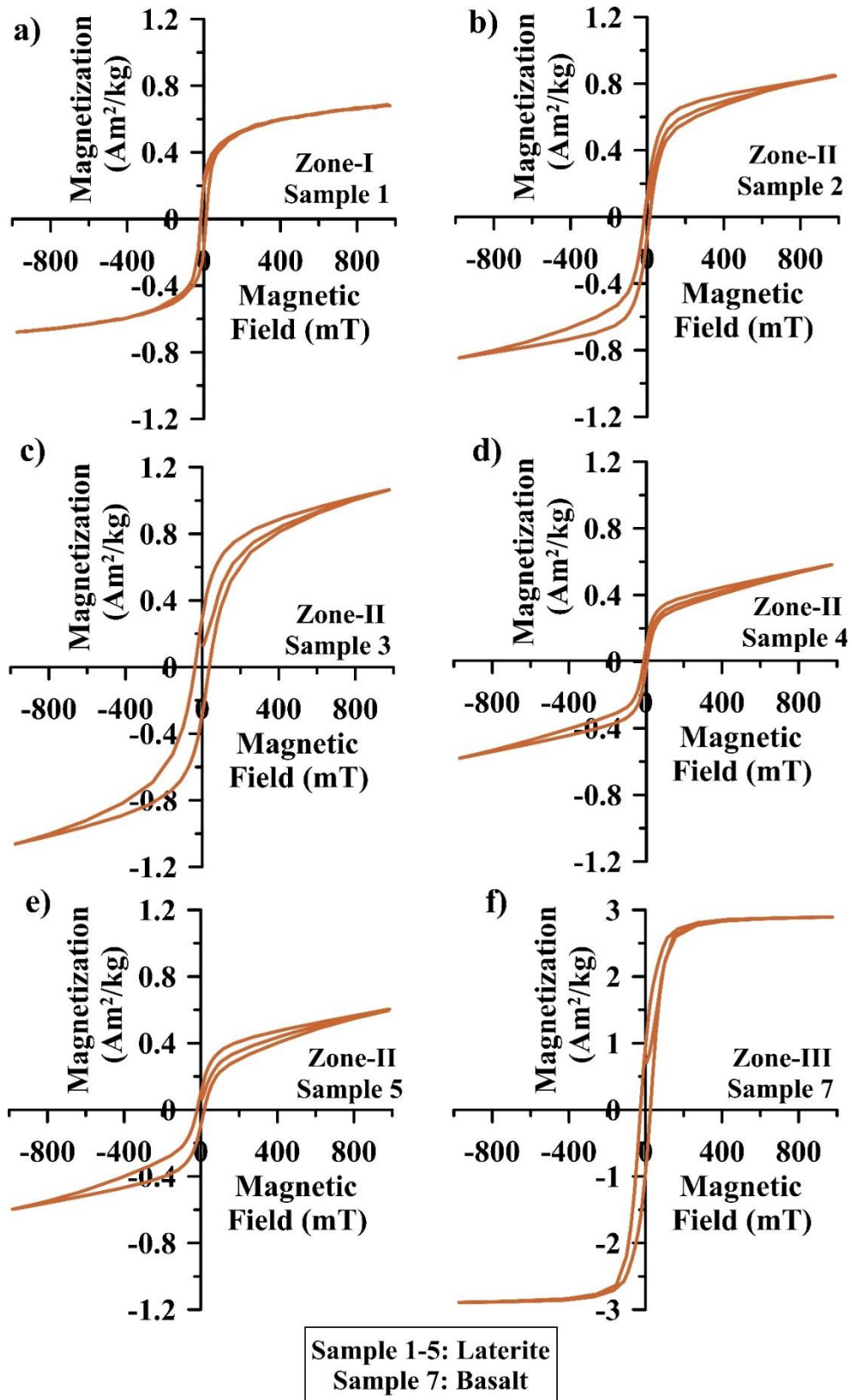


Figure 4

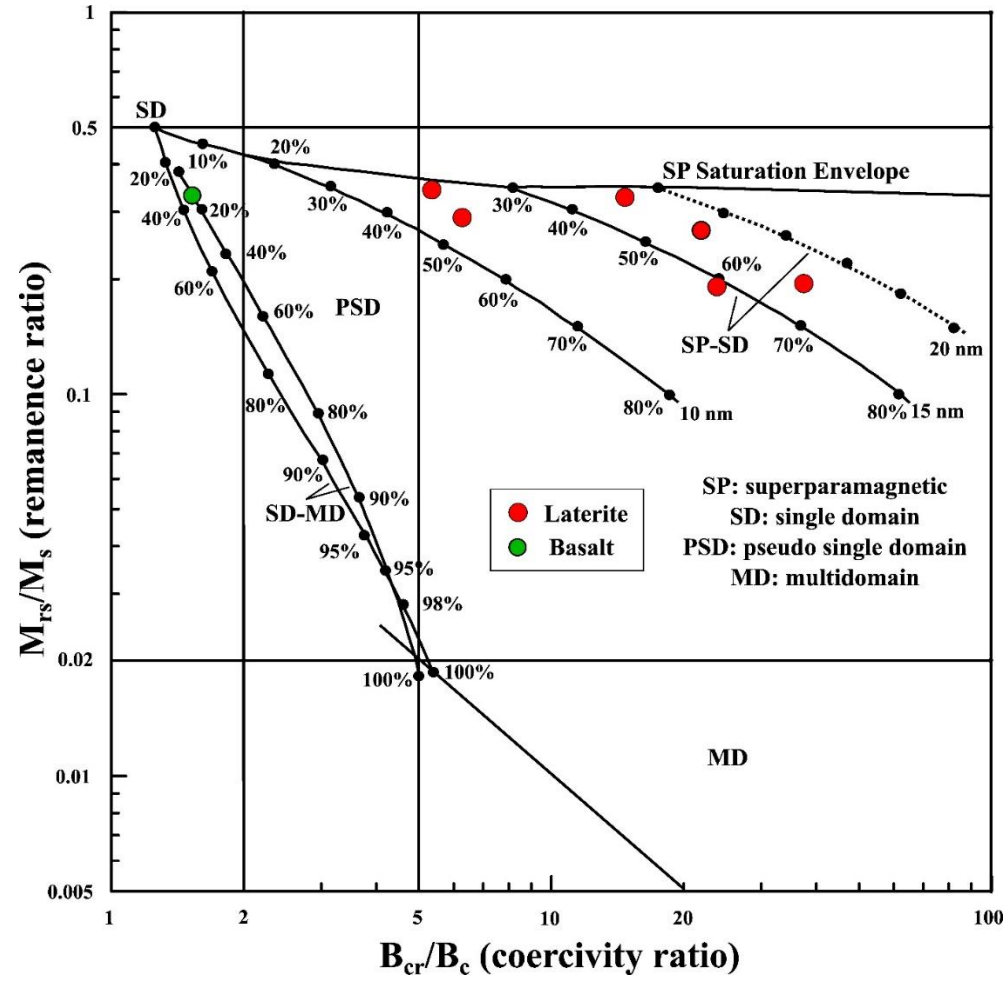


Figure 5

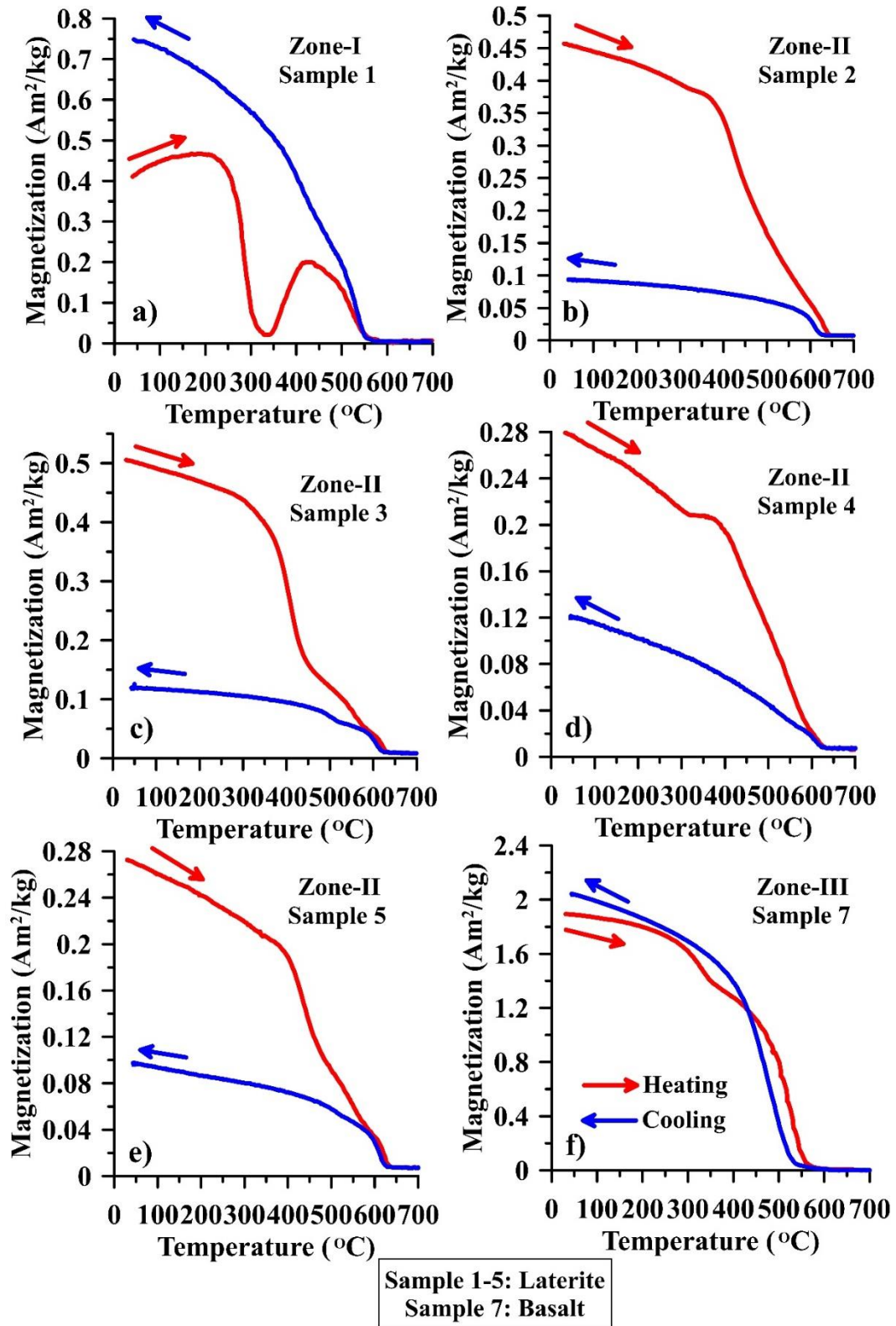


Figure 6



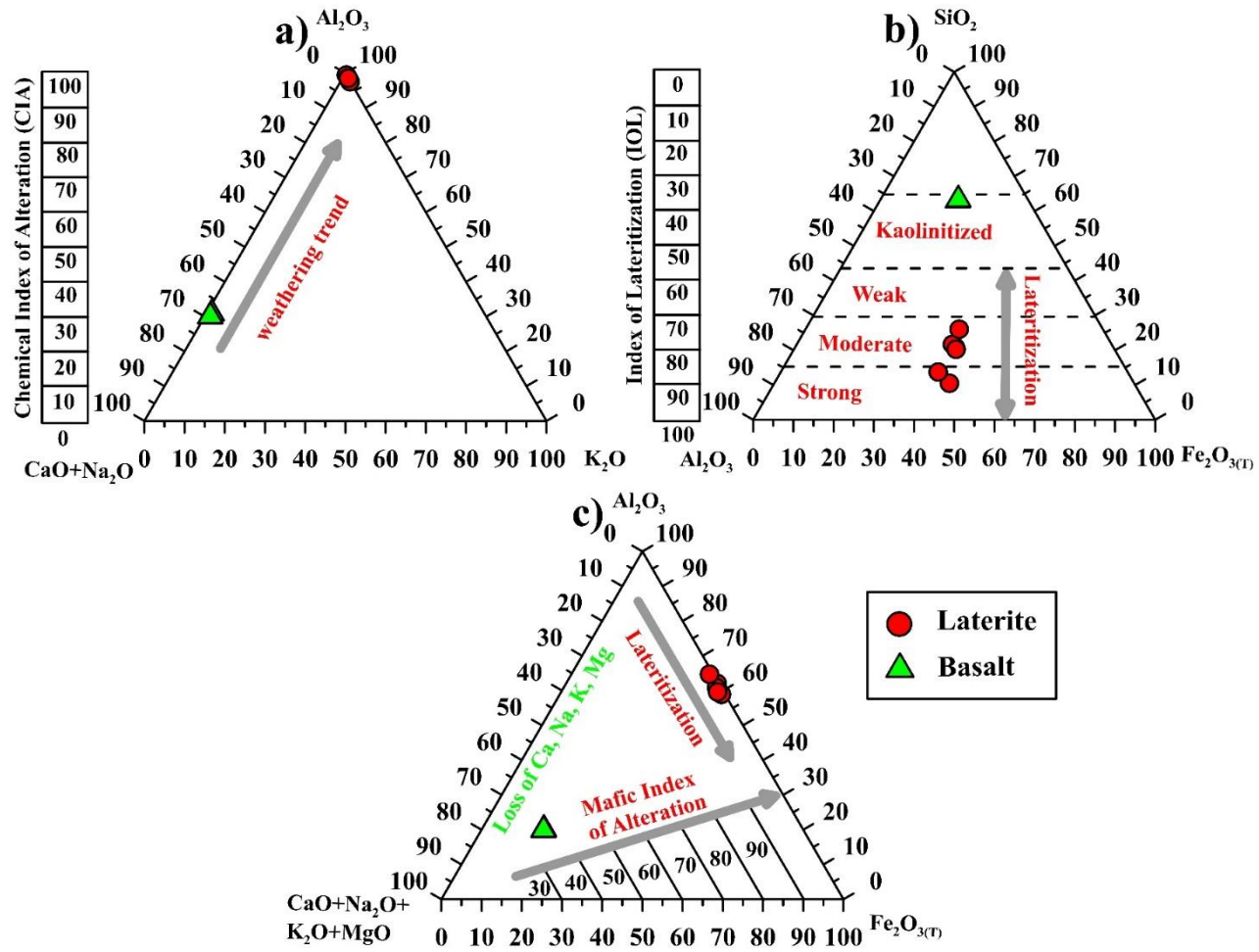


Figure 7

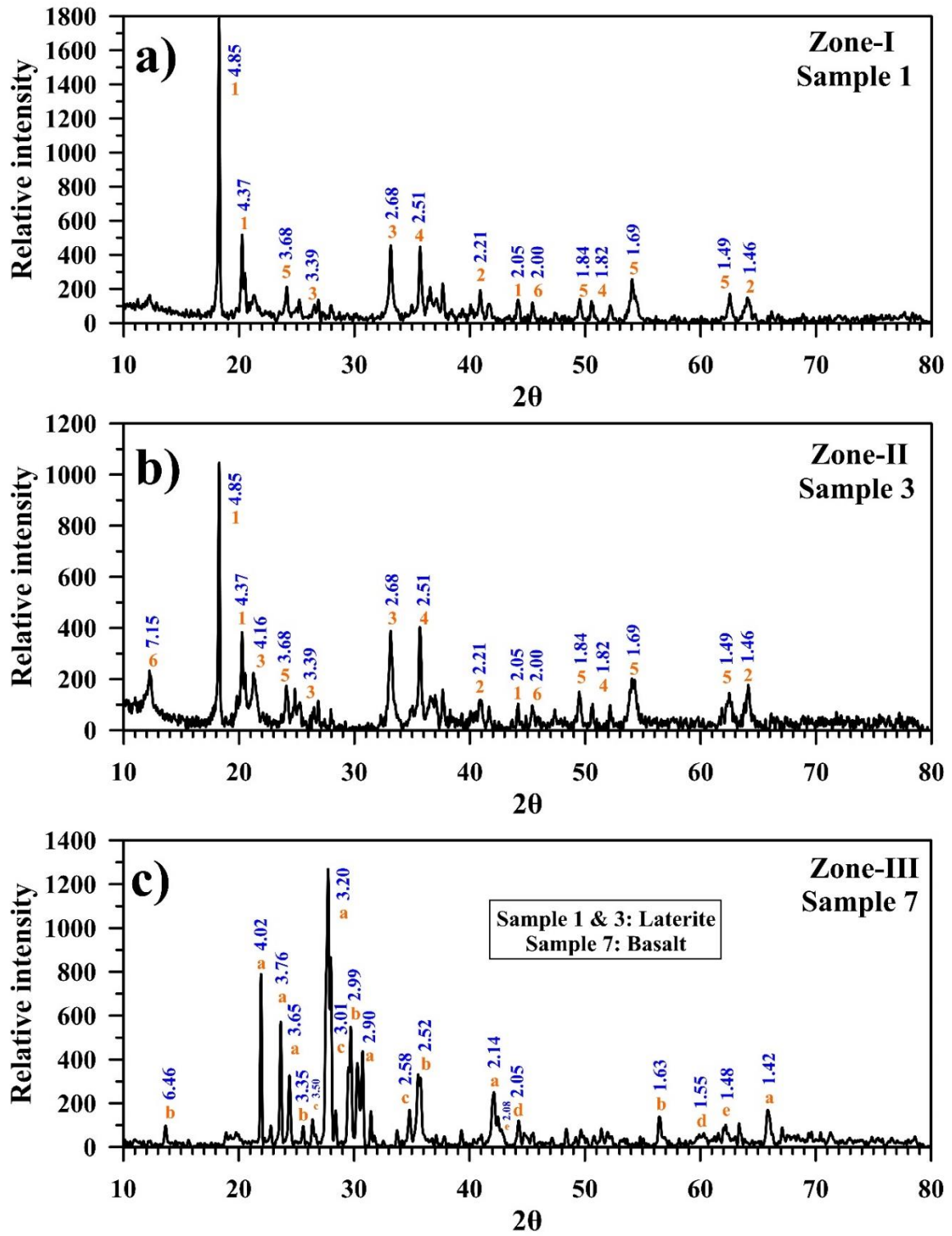


Figure 8

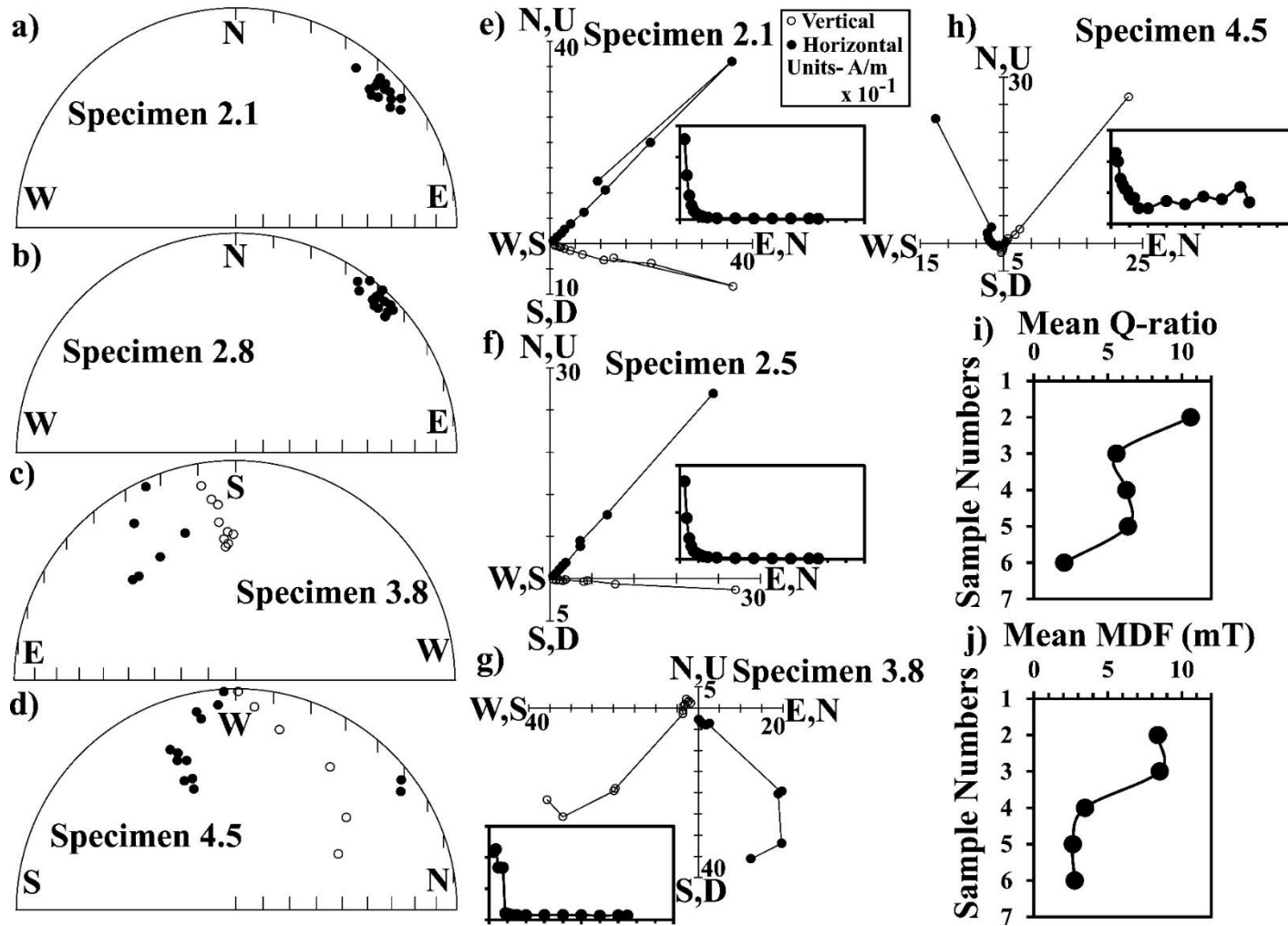


Figure 9

Table 1. Rock magnetic parameters and their formulae.

<b>Parameters</b>	<b>Formulae</b>	<b>References</b>
<b>S-ratio</b>	$\frac{\text{IRM}(-300\text{mT})}{\text{SIRM}}$	(King and Channel, 1991)
<b>Hard IRM</b>	$\frac{[\text{SIRM} + \text{IRM}(-300\text{mT})]}{2}$	(Robinson, 1986; Thompson and Oldfield, 1986)
<b>SoftIRM</b>	$\frac{[\text{SIRM} - \text{IRM}(-20\text{mT})]}{2}$	(Thompson and Oldfield, 1986)
<b>L-ratio</b>	$\frac{[\text{SIRM} + \text{IRM}(-300\text{mT})]}{[\text{SIRM} + \text{IRM}(-100\text{mT})]}$	(Liu et al., 2007)

Table 2. Rock magnetic parameters for laterite and basalt specimens (rounded to two decimal points). Units-  $\chi_{lf}$  ( $10^{-8}$  m<sup>3</sup>/kg),  $\chi_{ARM}$  ( $10^{-6}$  m<sup>3</sup>/kg), SIRM (Am<sup>2</sup>/kg), SIRM/ $\chi$  ( $10^8$  A/m), HIRM (Am<sup>2</sup>/kg), B<sub>cr</sub> (mT), Soft IRM (Am<sup>2</sup>/kg).

Specimen No./Parameters	$\chi_{lf}$	$\chi_{fd}\%$	$\chi_{ARM}$	SIRM	S-ratio	SIRM/ $\chi$		$\chi_{ARM}/\chi_{lf}$	HIRM	B <sub>cr</sub>	ARM/IRM 100	L-ratio	SoftIRM
1A	105.25	0.51	35.24	0.78	0.93	7.39		33.48	0.03	87.5	0.01	1.69	0.063
1B	92.09	0.71	33.27	0.85	0.96	9.18		36.12	0.02	100	0.01	1.91	0.034
1C	31.05	0.42	10.88	0.27	0.81	8.84		35.04	0.03	90	0.01	1.71	0.015
2A	2.07	4.52	0.17	0.03	0.68	15.21		8.33	0.03	575	0.02	0.85	0
2B	19.63	0.90	2.50	0.04	0.05	2.22		12.74	0.02	270	0.01	0.88	0.010
2C	39.91	0.59	4.85	0.08	0.16	1.98		12.14	0.03	175	0.01	1.09	0.019
3A	20.60	3.48	3.81	0.07	0.36	3.28		18.50	0.02	100	0.01	1.35	0.010
3B	9.35	5.47	2.48	0.05	0.23	5.59		26.56	0.02	165	0.01	1.08	0.007
3C	11.22	2.37	2.08	0.05	0.12	4.44		18.57	0.03	360	0.01	0.79	0.004
4A	35.85	0.41	3.35	0.03	0.02	0.94		9.33	0.02	320	0.02	0.85	0.008
4B	4.29	1.76	0.74	0.02	0.37	5.40		17.13	0.02	465	0.02	0.82	0.001
4C	6.95	1.67	1.28	0.03	0.04	4.10		18.40	0.02	325	0.01	0.78	0.003
5A	4.36	2.477	0.538	0.04	0.56	8.80		12.25	0.032	535	0.01	0.86	0.001
5B	21.90	0.767	2.71	0.06	0.05	2.61		12.36	0.03	325	0.01	0.80	0.008
5C	3.06	4.66	0.59	0.03	0.42	10.97		19.12	0.02	440	0.02	0.77	0.001
6A	4.63	0.97	0.78	0.03	0.33	7.01		16.86	0.02	430	0.01	0.77	0.001
6B	5.41	1.11	0.53	0.05	0.48	9.46		9.762	0.04	510	0.01	0.87	0.002
6C	17.58	0.56	3.31	0.08	0.31	4.30		18.84	0.05	450	0.01	0.87	0.006

<b>7A</b>	76.80	0.60	33.15	0.40	0.93	5.15		43.16	0.01	40	0.01	-	0.087
<b>7B</b>	84.06	1.54	37.99	0.46	0.92	5.47		45.19	0.02	41.25	0.01	-	0.094
<b>7C</b>	83.25	0.70	38.38	0.44	0.95	5.23		46.10	0.01	38.75	0.01	-	0.094
<b>7D</b>	81.91	0.43	36.28	0.43	0.97	5.17		44.29	0.01	40	0.01	-	0.086

Table 3. Chemical index of alteration (CIA), index of lateritisation (IOL) and mafic index of lateritisation (MIA) values for laterites (sample 1-6) and basalt (sample 7 & 8). Note that the XRF measurements were performed separately on the samples that were used for the rock and paleomagnetic studies, and the indices were calculated based on these measurements.

<b>Sample No./Alteration Index</b>	<b>Chemical Index of Alteration (CIA)</b>	<b>Index of Lateritisation (IOL)</b>	<b>Mafic Index of Alteration (MIA)</b>
<b>1</b>	100	89.5	100
<b>2</b>	99.3	79.3	99.6
<b>3</b>	99	78.3	99.4
<b>4</b>	99.4	74	99.6
<b>5</b>	98.3	79.7	99.3
<b>6</b>	99.7	86.3	99.8
<b>7</b>	32.6	36	36.7
<b>8</b>	31.8	35.7	36.4

Table 4. Koenisberger ratio (Q-ratio) for laterites (rounded to two decimal places).

<b>Specimen No.</b>	<b>Q-ratio</b>	<b>Sample No.</b>	<b>Mean Q-ratio</b>	<b>Standard Deviation</b>
<b>2.1</b>	5.14	<b>2</b>	10.59	13.37
<b>2.2</b>	8.13	<b>3</b>	5.58	2.27
<b>2.5</b>	2.54	<b>4</b>	6.25	1.66
<b>2.8</b>	5.14	<b>5</b>	6.35	5.25
<b>2.10</b>	4.94	<b>6</b>	2.04	0.77
<b>2.12</b>	37.64			
<b>3.1</b>	6.28			
<b>3.3</b>	2.55			
<b>3.5</b>	5.23			
<b>3.8</b>	9.45			
<b>3.10</b>	5.37			
<b>3.12</b>	4.62			
<b>4.1</b>	6.54			
<b>4.3</b>	6.84			
<b>4.5</b>	5.47			
<b>4.7</b>	9.12			
<b>4.10</b>	4.66			
<b>4.11</b>	4.86			
<b>5.1</b>	6.34			
<b>5.3</b>	1.38			
<b>5.5</b>	10.40			
<b>5.8</b>	2.44			
<b>5.10</b>	14.67			
<b>5.11</b>	2.86			
<b>6.1</b>	2.05			
<b>6.7</b>	1.59			
<b>6.5</b>	1.29			
<b>6.11</b>	1.95			
<b>6.10</b>	3.31			



Table 5. Median destructive field (MDF) of natural remanent magnetization (NRM) for laterites (rounded to two decimal places).

<b>Specimen No.</b>	<b>Median Destructive Field (mT)</b>	<b>Sample No.</b>	<b>Mean MDF (mT)</b>	<b>Standard Deviation</b>
<b>2.1</b>	13.56	<b>2</b>	8.37	5.13
<b>2.2</b>	3.85	<b>3</b>	8.50	4.54
<b>2.5</b>	11.95	<b>4</b>	3.45	0.70
<b>2.8</b>	3.85	<b>5</b>	2.63	0
<b>2.10</b>	13.56	<b>6</b>	2.76	0.45
<b>2.12</b>	3.46			
<b>3.1</b>	6.68			
<b>3.3</b>	14.77			
<b>3.5</b>	4.25			
<b>3.8</b>	13.56			
<b>3.10</b>	7.07			
<b>3.12</b>	4.68			
<b>4.1</b>	3.46			
<b>4.3</b>	3.85			
<b>4.5</b>	2.24			
<b>4.7</b>	3.85			
<b>4.11</b>	3.85			
<b>5.3</b>	2.63			
<b>5.8</b>	2.63			
<b>5.11</b>	2.63			
<b>6.7</b>	2.24			
<b>6.11</b>	3.02			
<b>6.10</b>	3.02			